Carbon compounds in the West Kimberley lamproites (Australia) : Insights from melt and fluid inclusions

Abersteiner, Adam

2022-09

Abersteiner , A , Golovin , A , Chayka , I , Kamenetsky , V S , Goemann , K , Rodemann , T & Ehrig , K 2022 , ' Carbon compounds in the West Kimberley lamproites (Australia) : Insights from melt and fluid inclusions ' , Gondwana Research , vol. 109 , pp. 536-557 . https://doi.org/10.1016/j.gr.20

http://hdl.handle.net/10138/346146
https://doi.org/10.1016/j.gr.2022.06.005

Gondwana Research 109 (2022) 536–557

Contents lists available at ScienceDirect

Gondwana Research

journal homepage: www.elsevier.com/locate/gr

Carbon compounds in the West Kimberley lamproites (Australia): Insights from melt and fluid inclusions

Adam Abersteiner [a,b,*], Alexander Golovin [c,d], Ivan Chayka [e], Vadim S. Kamenetsky [b,e,f], Karsten Goemann [f], Thomas Rodemann [f], Kathy Ehrig [g]

[a] Department of Geosciences and Geography, University of Helsinki, PO Box 64, FIN-00014, Finland
[b] Institute of Volcanology and Seismology, Petropavlovsk-Kamchatsky 683006, Russia
[c] V.S. Sobolev Institute of Geology and Mineralogy, Novosibirsk 630090, Russia
[d] Institute of the Earth's Crust, Siberian Branch, Russian Academy of Science, Irkutsk 664033, Russia
[e] Korzhinsky Institute of Experimental Mineralogy, Russian Academy of Science, Chernogolovka 142432, Russia
[f] Central Science Laboratory, University of Tasmania, Hobart, Tasmania 7001, Australia
[g] BHP Olympic Dam, Adelaide, South Australia 5000, Australia

ARTICLE INFO

Article history:
Received 2 November 2021
Revised 2 May 2022
Accepted 2 June 2022
Available online 6 June 2022
Handling Editor: S. Tappe

Keywords:
Lamproite
Melt inclusions
Ellendale
West Kimberley
Carbonate

ABSTRACT

Petrological and geochemical studies of lamproites can provide useful insights into the nature of their lithospheric mantle sources, but their geochemical and mineralogical diversity has complicated our understanding of their primary/parental melt composition, volatile (CO_2, H_2O) inventory and magmatic evolution. To help address this issue, we present a detailed study of different generations (primary, pseudosecondary, secondary) of crystal, and melt and fluid inclusions in olivine, Cr-spinel and perovskite from three olivine lamproites in the Ellendale Field of the West Kimberley Province (Australia) in order to understand the composition and evolution of their parental magmas.

Melt inclusions in the different host minerals and from each of these localities are broadly similar to each other and consist of glass, alkali/alkali-earth (Mg-Ca-K-Na-Ba) carbonates, phosphates and chlorides, in addition to minerals typical of lamproite groundmass (fluorapatite, perovskite, phlogopite, diopside, wadeite, Mg-ilmenite, Fe-Mg-Ti-Cr spinel). The dominant volatile species in the melt and fluid inclusions is CO_2 based on Raman data. Heating experiments of melt/fluid inclusions in olivine show significant phase transformations in which the carbonate may separate into an immiscible carbonate-rich sulphate-bearing fraction or exsolve a CO_2 fluid.

Our results indicate that carbonates, along with alkali/alkali-earths, halogens and sulphur, became progressively concentrated in the West Kimberley lamproitic magmas during crystallisation, leading to the entrapment of a complex array of daughter minerals, some not previously reported from lamproites and, in some inclusions, immiscible carbonate melt. The widespread occurrence of daughter carbonates in melt/fluid inclusions in lamproite minerals is at odds with their apparent paucity in the lamproite groundmass. The presence of carbonate and the abundance of CO_2-rich and H_2O-poor melt and fluid inclusions are attributed to the preferential partitioning of CO_2 into the vapour and retention of H_2O in the magma during degassing, coupled with H_2O loss by post-entrapment modification of the inclusions through H^+ diffusion.

1. Introduction

Lamproites constitute a group of rare ultrapotassic ($K_2O/Na_2O > 2$), Mg-rich igneous rocks that are generally characterised by low CaO and Al_2O_3 contents, and strong enrichments in incompatible trace elements (e.g. Foley et al., 1987; Mitchell and Bergman, 1991; Mitchell, 2020). Lamproite occurrences have been documented on all continents and range widely in emplacement age from Archean (~2.7 Ga; Sergreev et al., 2007) through to Quaternary (~56 ka; Tingey et al., 1983). Lamproites globally exhibit a wide range in chemical and radiogenic Sr-Nd-Pb-Hf isotope compositions, which is dependent on their geodynamic setting (e.g., 'orogenic' vs. 'anorogenic'; e.g., Mitchell and Bergman, 1991; Prelević et al., 2010; Lustrino et al., 2016; Mitchell, 2020). The

* Corresponding author at: Department of Geosciences and Geography, University of Helsinki, PO Box 64, FIN-00014, Finland.
E-mail address: adam.abersteiner@helsinki.fi (A. Abersteiner).

https://doi.org/10.1016/j.gr.2022.06.005
1342-937X/

melts that give rise to lamproites are considered to have originated from low-degree partial melting of metasomatically enriched subcontinental lithospheric mantle containing significant quantities of titanian phlogopite and K-titanian richterite (Jaques et al., 1984a; Foley, 1992; Mitchell, 1995b, 2020; Davies et al., 2006; Jaques and Foley, 2018). The potential wide variability in the lithospheric mantle source composition and volatile (C-O-H) contents, and depths of magma generation is thought to be responsible for the diversity in mineralogy (e.g., olivine-rich vs. leucite-rich lamproites vs. carbonate-bearing), geochemistry and isotopic composition (Foley et al., 1987; Mitchell and Bergman, 1991; Mitchell, 2020) of lamproite rocks. Thus, these variations in lamproites present numerous complications when attempting to reconstruct parental melt compositions and petrogenetic models. Furthermore, many lamproites, especially high MgO (e.g., ~22–24 wt% - based on estimates from olivine-liquid equilibria; Jaques and Foley, 2018) olivine-bearing varieties, commonly contain abundant mantle xenocrysts (Foley, 1993; Mitchell, 1995b). Therefore, the bulk compositions of such rocks cannot be accurate representations of the original lamproite melts that formed in the mantle. Recently, attempts have been made to redefine lamproites and to incorporate rocks formerly termed 'orangeites' (or 'Group-II kimberlites'; see Smith, 1983; Mitchell, 1995a), which have now been considered to be a carbonate-rich variety of lamproite (see Dawson, 1987; Pearson et al., 2019). Similar to lamproites, these rocks exhibit a wide range of enriched Sr–Nd–Hf isotopic compositions and are thought to have formed by similar processes, however, their reclassification as a variety of lamproite has proven controversial (see Tappe et al., 2022).

Analyses of melt and fluid inclusions entrapped in minerals have been applied extensively and are invaluable tools in the study of igneous rock petrogenesis (e.g., Kent, 2008; Métrich and Wallace, 2008). After entrapment, melt and fluid inclusions are potentially isolated from external modification and thus can provide valuable insights into the attributes of melts and fluids during different stages of magmatic evolution, including prior to processes such as eruption, devolatisation and crystallisation (e.g., Lowenstern, 2003). In this study, we provide a comprehensive review of crystal, melt and fluid inclusion data from lamproitic minerals from localities worldwide (Table 1), as well as present a systematic study of different generations (primary, psuedosecondary, secondary) of crystal and of melt and fluid inclusions hosted in olivine, Cr-spinel and perovskite from three diamondiferous lamproites (E4, E9 and E11) from the Ellendale Field of the West Kimberley lamproite province (Western Australia). In contrast to the carbonate-poor nature of lamproite rocks in this location, our results demonstrate that carbonates are common daughter phases within melt/fluid inclusions. Here, we discuss the significance of melt/fluid inclusion compositions in lamproite minerals and their implications for lamproite magma evolution in the West Kimberley lamproite province.

2. Melt inclusions in lamproites and other potassic alkaline Rocks: Background

Melt inclusions in magmatic minerals are powerful petrological tools for examining the nature of magmas parental to igneous rocks. In examination of potassic alkaline rocks, melt inclusions have been applied to obtain insights into parental melts of various types of these rocks. For example, studies of kimberlite minerals showed that their inclusions contain appreciably high amounts of carbonates and may even approach high-halogen and alkaline-bearing carbonatitic compositions with minor silica (e.g., Kamenetsky et al., 2013, 2014; Abersteiner et al., 2018, 2019), thereby providing additional evidence to support their originally carbonate nature. However, the application of information obtained from melt inclusions to the origin and evolution of other potassic rocks appear less widely utilized than in kimberlites, despite the existence of numerous studies of melt inclusions in minerals from lamproites, kamafugites and other exotic potassic rocks (see Table 1; Supplementary Table S1).

The earliest studies noticed that leucite from lamproites of the West Kimberley province (Australia) is populated by abundant solid inclusions (Wade and Prider, 1940). Ensuing detailed studies showed that the inclusions do not occur only in leucite, but also in olivine, diopside and other rock-forming minerals, and are comprised of crystals (e.g., pleonaste-hercynite, chromite), and glasses that were interpreted to represent entrapped and quenched melts (Jaques and Foley, 1985; Sobolev et al., 1989; Sharygin, 1991; Hwang et al., 1994) or immiscible silicate melts (Mitchell, 1991). These melt inclusions in lamproite minerals were thought to be proxies of the parental melt, and were found to contain higher abundances of Na, Sr, Ba and Zr than the host rocks and exceptionally high F-contents (up to 1.4 wt%; Sobolev et al., 1985). Homogenisation temperatures of the olivine-hosted melt inclusions (with ~8–9 wt% MgO) in lamproites varied between 950 and 1050 °C (Sobolev et al., 1989). These studies found high contents of nearly pure CO_2 in the fluid phase of these inclusions which was considered to be at odds with the proposed low activity of CO_2 in lamproite magmas (Jaques et al., 1984a; Foley, 1989). These results prompted suggestions that the melting regimes and parental melts of lamproites and kimberlites might be similar, with the most notable differences in Ca, Al and F contents (Sobolev et al., 1985, 1986; Ryabchikov et al., 1986). According to this scenario, the low content of carbonate in lamproite rocks compared to that of kimberlites was attributed to the Ca-poor composition of the lamproite melts, which precluded the immobilization of CO_2 during magmatic process (Sobolev et al., 1985, 1989). These findings were supported by studies of melt inclusions from lamproites of the Mediterranean province (Murcia-Almeria; Sharygin, 1997), North America (Smoky Butte, Leucite Hills, Prairie Creek; Solovova et al., 1989; Sharygin, 1997) and Antarctica (Gaussberg; Salvioli-Mariani et al., 2004), which also found a high activity of CO_2, along with H_2O and N_2.

Homogenization experiments, performed on the melt inclusions from these occurrences (with varying MgO ~ 1–10 wt%) from, and experimental studies (using MgO ~ 8 wt%) on lamproites (Foley, 1985), showed that liquidus temperatures, at which point inclusions began to crystallize, typically occurred around ~1200 °C (Sobolev et al., 1975; Solovova et al., 1988, 1989; Sharygin, 1991, 1997; Salvioli-Mariani and Venturelli, 1996; Salvioli-Mariani et al., 2004). Importantly, it was also found that melt inclusions in lamproite minerals from Leucite Hills and Smoky Butte contain carbonates (e.g., calcite) and unidentified salt phases (Sharygin, 1997, 1998).

Melt inclusion studies on the lamproite occurrences within the Mesozoic Aldan potassic province (Central Siberia) provided further evidence for an important role of carbonate in lamproite petrogenesis. In a wide variety of occurrences, carbonates (including Sr-bearing calcite) and salts (Ca-Na-K chlorides) occur as typical daughter minerals in melt inclusions (both glassy and fully-crystallized) in lamproite phenocrysts (olivine, clinopyroxene, Cr-spinel, apatite), where upon heating, significant parts of the inclusions exhibited silicate-carbonate immiscibility (Panina and Vladykin, 1994; Panina and Konev, 1995; Panina and Motorina, 2008; Rokosova and Panina, 2013). Lamproites of the Mesozoic Murun alkaline complex (Aldan-Stanovoi Shield, Siberia) provided the best example of this feature with multiple populations of inclusions in different minerals being represented by pure-silicate, silicate alkali-carbonate and alkali-carbonate assemblages with various concentrations of halides (Panina and Vladykin, 1994).

Table 1
Summary of inclusion data from lamproite minerals from localities worldwide listed in order of relative publication chronology (oldest to newest).

Reference	Location	Host Mineral	Type of Inclusion	Daughter Phases	Temperature(s) of homogenisation (°C)
Wade and Prider (1940), Jaques et al (1984a), Jaques et al. (1986), Stachel et al. (1994)	West Kimberley, Australia	Olivine	Crystal and melt	Chromite, melt	
		Phlogopite	Crystal	Olivine, chromite, diopside, perovskite, leucite, apatite, priderite, wadeite, barite	
		Diopside	Melt		
Jaques (2016) Jaques and Foley (2018), Hwang et al. (1994)		Potassium richterite	Crystal	Olivine, diopside, perovskite, leucite, apatite, priderite, phlogopite, wadeite, barite	
		Perovskite	Crystal and melt	Olivine, chromite, melt	
		Wadeite	Crystal	Chromite	diopside, perovskite, apatite
Jaques and Foley (1985), Jaques et al. (1986), Hwang et al. (1994), Stachel et al. (1994)	West Kimberley, Australia	Leucite	Crystal	Pleonaste-hercynite	
Jaques and Foley (1985)	West Kimberley, Australia	Leucite	Crystal	Pleonaste-hercynite	
Sobolev et al. (1985), Sobolev et al. (1989) **Sobloev et al. (1989)**	Ellendale (E4, E7, E9, E11) Mt Cedric (Western Kimberley, Australia)	Olivine	Fluid	Dominantly CO_2 and minor N_2, H_2O	
			Melt	Kalsilite, F-bearing Ti-phlogopite, picroilmenite, F-apatite, F-bearing K-richterite, perovskite, residual glass, fluorite(?)	950–1100
			Melt/Fluid	Orthopyroxene + dense fluid, orthopyroxene + K-richterite, residual glass + high/low density CO_2 fluid	
			Crystal	Chromite, orthopyroxene	
Ryabchikov et al. (1986)	Ellendale (E11), Australia	Olivine	Crystal	Olivine + orthopyroxene + chromite + clinopyroxene	950–970
Solovova et al. (1988)	Almeria, Murcia, Albacete (Spain)	Olivine	Melt + crystal + fluid	Glass + (olivine + phlogopite + sanidine + apatite) + fluid	1050–1250
		Clinopyroxene	Crystals + melt(?) + fluid(?)		820–1100
		Phlogopite			1040–1140
		Sanidine			940–1100
		Apatite			1040–1160
		Carbonate	Melt + crystal + gas + liquid		
Solovova et al. (1989)	Prairie Creek, USA	Olivine	Melt	Diopside, sphene, perovskite, richterite	1000–1050
			Crystal	Spinel, ilmenite	
			Fluid	$CO_2 > H_2O$	
Sharygin and Bazarova (1991), Sobolev et al. (1975)	Leucite Hills, USA	Phlogopite	Melt + gas ± crystals	Glass + gas + leucite + ore phases + unidentified transparent phases	1240–1270
		Diopside	Melt + gas + crystals	Glass + gas + leucite + K-feldspar + unidentified transparent phases	1220–1270
		Leucite	Melt	Glass ± gas	1150–1250
		Apatite	Melt + gas + crystals	Glass + barite + ore phases + unidentified transparent phases	>1150
Mitchell (1991)	Oscar (West Kimberley, Australia) Zirkel Mesa, Leucite Hills (USA)	Leucite	Glass	Glass	
Sharygin (1991)	Ellendale (E5)	Phlogopite	Melt	Glass + gas	1130–1200
	Ellendale (E5)	Apatite	Melt, Melt/Fluid, Fluid	Glass + gas, pyroxene(?)	
	Ellendale (E11)	Olivine	Melt Type 1: Glass + ore + crystals + gas		1030–1050, 990–1050
	(Western Kimberley, Australia)		Melt Type 2: Glass + gas		
			Combined fluid inclusions	CO2, phlogopite, kalsilite, diopside	970–990
Venturelli et al. (1993)	Jumilla, Spain	Apatite*	Primary Melt/ Fluid	Halite, Sylvite, K_2SO_4, low density gas	
		Post-magmatic apatite-hematite-carbonate veins	Secondary (to pseudosecondary) Melt/Fluid	Halite, Sylvite, K_2SO_4, $FeCl_2$, Mg-chloride, K-Ca-sulphate, $MgSO_4$	630–700
Sharygin (1993)	Ryabinovi, Russia	Olivine	Glass + crystals	Glass + phlogopite + leucite + richterite + ore phase + gas	>1250–1300
		Clinopyroxene	Crystal	Phlogopite + Kfeldspar + garnet (grossular-andradite)	1200–1240
Panina and Vladykin (1994)	Murun, Russia	Pyroxene	Melt + crystals	Glass + silicates + ore phases + gas	1235–1270
			Salts (secondary)	Salts + gas	~920
		Apatite	Melt + crystals	Glass + silicates + ore phases + gas	1250–1280

Table 1 (*continued*)

Reference	Location	Host Mineral	Type of Inclusion	Daughter Phases	Temperature(s) of homogenisation (°C)
			Melt + salts	Glass + salts + gas	800 (two liquids)
			Salts	Salts + gas	750–800
		K-feldspar	Melt + salts	Glass + salts + gas	600–650 (two liquids and gas)
			Salts	Glass + salt + gas	750 (liquid + gas)
		Olivine	Melt	Glass + ore phases + clinopyroxene + phlogopite + feldspar + arfvedsonite	not homogenized due to darkening of the host
Panina and Konev (1995)	Molbo, Russia	Apatite	Melt/Melt + Crystal	Glass + magnetite + phlogopite + K-feldspar + Na-K-sulphate	1030–1150
		Clinopyroxene	Melt + crystal	Glass + olivine + leucite + gas	1180–1240
Salvioli-Mariani, E., and Ventirelli, G. (1996)	Jumilla, Cancarix (Spain)	Olivine	Glass,	Cr-spinel	>1170–1200
		Clinopyroxene	Fluid ± Crystal	Sanidine, leucite, analcime	1100–1150
		Apatite		Leucite	1020–1170
		Sanidine		Phlogopite, analcime	830–1055
		K-richterite			990–1150
		Phlogopite			725
		Pseudobrookite			
Panina et al. (1996)	Yakokut, Russia	Olivine	Melt?		1440–1420
		Pyroxene	Melt?		1285–1220
Sharygin (1997)	Ellendale (E11), Australia	Olivine	Melt/Fluid	High density fluid, phlogopite, orthopyroxene, kalsilite	
			Crystal	Chromite, orthopyroxene ± glass/fluid	
	Ellendale (E5), Australia	Phlogopite/ Apatite	Melt, Melt/Fluid, Fluid	Glass + gasm diopside.	
	Wolgidee Massif (Western Australia)	Diopside	Melt	Glass + gas, phlogopite	
	Wyomingite (Leucite Hills, USA)	Phlogopite, Diopside, Apatite	Melt	Glass, Glass + Gas ± crystals, Cr-rich olivine, barite, apatite, kalsilite, salts(?)	
	Murcia-Almeria (Spain)	Olivine	Melt	Glass + gas + crystals, phlogopite, diopside, sanidine	
	Smoky Butte (USA)		Melt	Glass + gas + crystals, armalcolite, apatite, diopside, priderite, calcite	>1200
			Crystal	Cr-spinel, sulphides (pentlandite, chalcopyrite)	>1250
		Diopside, Apatite, Phlogopite	Melt Crystal	Glass + gas, sanidine Apatite, armalcolite, leucite	
Panina et al. (1998)	Coc Pia, Vietnam	Clinopyroxene (phenocryst cores)	Melt + crystal + gas (high-Mg)	Glass + K-Feldspar + phlogopite + magnetite	1230–1240
		Clinopyroxene (phenocryst rims)			1170–1210
		Clinopyroxene (groundmass)			1195–1220
		Olivine		Glass + silicates + ore phases + gas	1240–1265
		Apatite	Melt + gas (high-Mg)	Glass + gas	
		Clinopyroxene, olivine, phlogopite	Melt + gas (syenitic)	Glass + gas + rare crystals (magnetite, apatite, plagioclase)	1060–1100
		Clinopyroxene, apatite	Crystal + gas (carbonate)	Carbonates + ore phases + gas	
Sharygin et al. (1998)	Smoky Butte, USA	Olivine	Melt	Glass + armalcolite + crystals (apatite, diopside) + gas + salts/carbonates, sulphides	>1250
		Apatite	Melt	Glass	1220–1230
		Diopside	Melt	Glass + gas	1160–1205
		Phlogopite	Melt	Glass + gas	1085–1210
Sharygin et al. (2003)	Smoky Butte (USA)	Olivine	Sulphides + Melt/ Fluid	Pentlandite, chalcopyrite, monosulphide solid solution + chalcopyrite, violarite	
			Crystal	Cr-spinel	
	Leucite Hills (USA)		Sulphides + Melt/ Fluid	MSS + pentlandite, MSS + chalcopyrite	
			Crystal	Cr-spinel	
	Fortunite (Spain)	Orthopyroxene	Sulphides + Fluid + Oxides	pentlandite, heazlewoodite, pentlandite, pyrrhotite, godlevskite, Fe-oxide	
		Phlogopite			
Salvioli-Mariani et al. (2004)	Gaussberg, Antarctica	Olivine	Melt/Fluid	Silicate melt - glass, CO_2 fluid	Not homogenised: Final temperature of melting 1070–1140
		Leucite			
		Clinopyroxene	Melt/Fluid	Silicate melt - glass, phlogopite, CO_2 fluid	
Panina (2005)	Yukhta, Russia	Clinopyroxene	Crystal	Magnetite	

(*continued on next page*)

Table 1 (*continued*)

Reference	Location	Host Mineral	Type of Inclusion	Daughter Phases	Temperature(s) of homogenisation (°C)
				K-feldspar	
				Biotite	
			Melt	Glass + K-feldspar + plagioclase + magnetite + biotite + gas	1190–1205
		Olivine	Crystal	Biotite	
			Melt	Glass ± K-feldspar + biotite + apatite + opaque phase	1000–1050
Rokosova and Panina (2013)	Ryabinoviy, Russia	Clinopyroxene	Silicate (crystals)	Clinopyroxene + biotite + albite + rutile	1120–1190
			Silicate-carbonate (crystals)	Clinopyroxene + biotite + ankerite + rutile	
			Carbonate-salt (crystals + liquid + gas)	Calcite + K-Na-chlorides + Sr-Ca-sulphate + titanite + liquid + gas	
			Carbonate (crystals)	Calcite + portlandite	
Chayka et al. (2018) Chayka et al. (2020)	Ryabinoviy, Russia	Olivine-1	Crystal + fluid/gas	Phlogopite + clinopyroxene + calcite + apatite + sulphides	1250–1350
		Olivine-2	Crystal	Na-phlogopite + monticellite	1250–1350
		Chromite	Crystal	Phlogopite + diopside + olivine + apatite + sulphides + calcite	~1300 (unpublished)

Importantly, abundant carbonates and sulphates in inclusions within potassic rocks (including lamproites) of the Malyi intrusion in the Murun complex and close spatial association of these rocks with carbonatites allowed for the suggestion that silicate-carbonate immiscibility, recorded in these inclusions, was responsible for the carbonatite formation (Panina and Usol'tseva, 1999, 2000). This hypothesis was corroborated by melt inclusion studies performed on other alkaline occurrences (including high-potassic), summarized in Panina and Motorina (2008).

Therefore, there is a considerable amount of data on melt inclusions in lamproite minerals showing that these melts contain carbonate, which is considered to become enriched after extensive crystallisation of the lamproite magma and may remobilize due to either devolatilization (Sobolev et al., 1989; Salvioli-Mariani et al., 2004) or silicate-carbonate immiscibility (Panina and Vladykin, 1994; Panina and Motorina, 2008; Rokosova and Panina, 2013).

3. Background Geology

The lamproites examined in this study are from the West Kimberley lamproite province, which lies at the southwest margin of the Kimberley Craton of Western Australia, extending from the Proterozoic King Leopold Orogen bordering the craton across the Fitzroy Trough in the northern Canning Basin (Fig. 1). This major lamproite province comprises ~180 individual volcanic pipes, plugs, sills and dykes clustered in three main fields with a few isolated smaller volcanic centres in Fitzroy Valley and the Lennard Shelf to the north (Jaques et al. 1984a, 1986). The southernmost Noonkanbah field is dominated by leucite lamproite plugs and pipes with minor olivine lamproite occurrences (Prider, 1939, 1959; Wade and Prider, 1940). For detailed descriptions on the geology, petrography and compositions of the E4, E9 and E11 lamproites and other West Kimberley lamproites, the reader is referred to Jaques et al. (1986) and Stachel et al. (1994). The northernmost Ellendale field is dominated by largely buried volcanic pipes of olivine lamproite discovered by diamond exploration in the mid-to late 1970's (Smith and Lorenz, 1989) together with a small number of leucite lamproite pipes and plugs (Jaques et al., 1986). The smaller Calwynyardah field, in between the two previous volcanic areas, comprises mainly buried volcanic pipes filled with pyroclastic olivine lamproite and olivine leucite lamproite. Many of the Ellendale pipes carry diamonds at low concentrations (mostly < 1 carats per hundred tonnes; cpht). Two of the pipes with the highest grades (4–14 cpht; Ellendale 9 (2002–2015) and Ellendale 4 (2005–2009)) have been mined producing>2.1 million carats (Ahmat 2012). The lamproites are all of Miocene age with K–Ar and Ar–Ar ages ranging from ~21–22 Ma in the north to ~17–20 Ma in the Noonkanbah field in the south (Wellman, 1973; Jaques et al., 1984b; Phillips et al., 2012).

4. Analytical methods

Lamproite specimens were prepared as thin sections, and rock chips and olivine grain separates, which were mounted in epoxy resin, and polished using kerosene as lubricant to avoid dissolution of any water-soluble minerals (with the exception of thin sections, which were polished using water). Optical examination of the samples was performed on a Nikon Eclipse 50i POL microscope at the University of Tasmania. The identification and composition of daughter phases within both unheated and heated inclusions were examined using field emission scanning electron microscopy equipped with an energy-dispersive X-ray spectrometer and Raman spectroscopy (see sections below).

Heating experiments were performed first by separating olivine grains from crushed lamproite rock samples. The separated olivine grains were then placed in a muffle furnace at 1050 °C for 5 min and quenched after removal. To avoid oxidation, olivine grains were wrapped with graphite in Pt foil. They were subsequently mounted and polished in epoxy resin. The temperature and duration of heating was designed to achieve homogenization of the melt/fluid inclusions and the selected temperature was based on previous studies of heating and homogenization of olivine-hosted melt/fluid inclusions in lamproites (e.g., Sobolev et al., 1989; Sharygin, 1991; Salvioli-Mariani et al., 2004; see also Table 1). Noteworthy is that not all inclusions homogenized completely, as melt + crystals (e.g., apatite, perovskite) were produced (see results section).

Detailed studies of groundmass phases and inclusions in minerals were performed using a Hitachi SU-70 field emission (FE) scanning electron microscope (SEM) equipped with an Oxford AZtec XMax 80 detector at the Central Science Laboratory, University of Tasmania. Energy-dispersive X-ray spectrometry (EDS) semi-quantitative analyses and backscattered electron (BSE) images

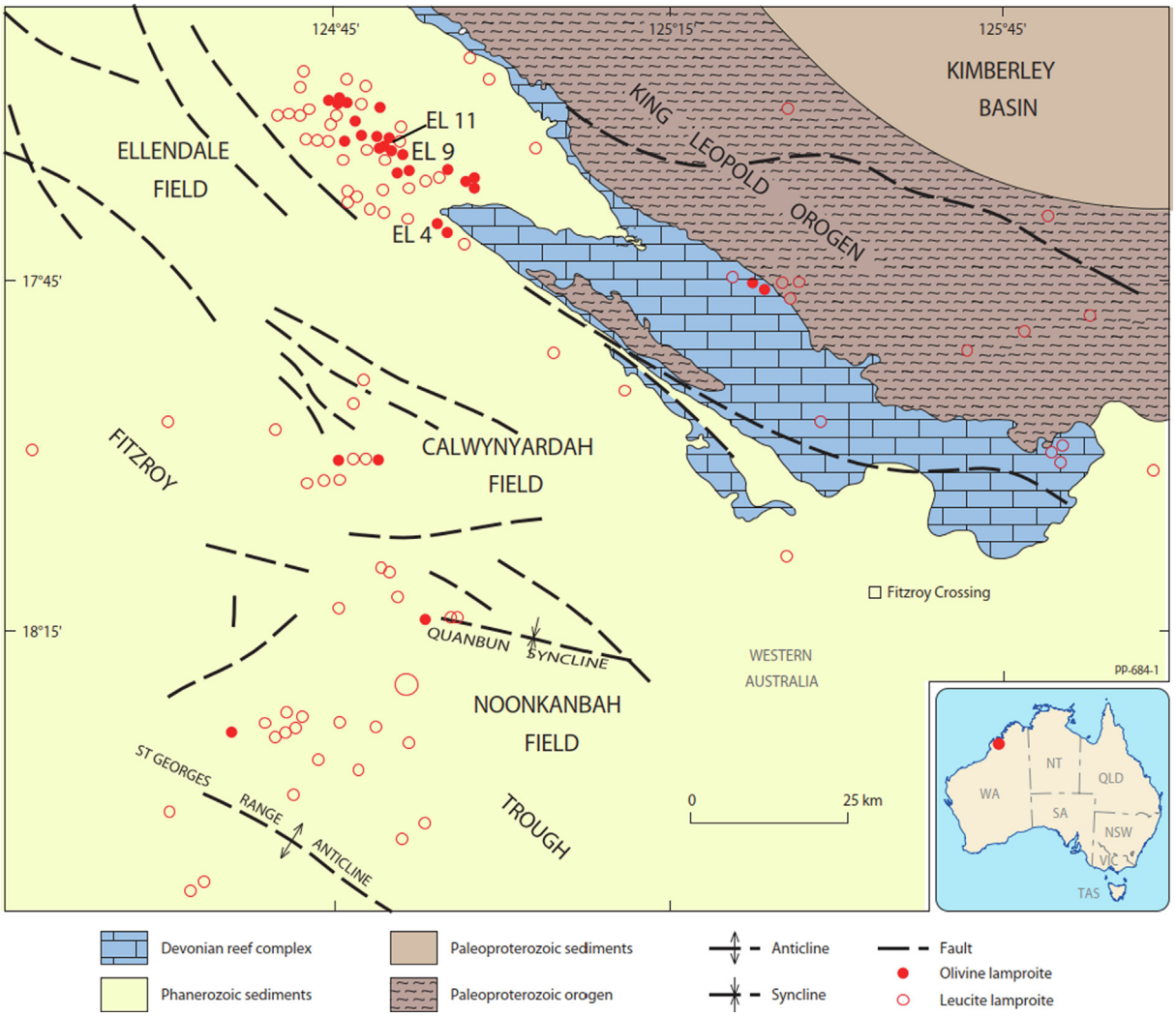

Fig. 1. Geological map showing the distribution of lamproite intrusions in the West Kimberley Province (Western Australia) and the locations of E4, E9 and E11. **Fig.** modified after (Jaques et al. 2016).

were collected with an accelerating beam voltage of 15 kV, beam current of 3nA and acquisition time of 10–20 s and an Oxford Instruments INCA Energy 350 microanalysis system with EDS XMax-80 Silicon Drift Detector installed on a JEOL JSM-6510LV SEM at the Sobolev Institute of Geology and Mineralogy (SB RAS, Novosibirsk). EDS spectra and BSE images were collected with an accelerating voltage of 15 kV, beam current of 1nA and acquisition time of 60 s. Minerals were identified using compositions obtained by SEM-EDS and the compositional database of the MinIdent-Win 4 software package (formerly Micronex, Canada). The compositions of daughter minerals and glasses within inclusions were too small to reliably analyse.

The major and trace element compositions of olivine were measured at the Central Science Laboratory (University of Tasmania) using a JEOL JXA-8530F Plus field emission electron microprobe. The following conditions were employed: a beam with an accelerating voltage of 15 kV, a beam current of 300nA and beam size of 2 μm. The WDS on peak and off peak counting time was 60 s for Al, Cr, Ca, Mn and Ni. Mg, Fe and Si were analyzed simultaneously using a Thermo Pathfinder UltraDry EDS system. The calibration standards were olivine San Carlos NMNH 111312-44 for Mg, Fe and Si, corundum Harvard for Al, wollastonite UNE for Ca, eskolaite for Cr, rhodonite for Mn, and nickel oxide for Ni. Detection limits (99% confidence) were < 0.004 wt% for Al, Cr, Ca, Mn and Ni.

The Raman spectra of daughter phases in olive-hosted melt/fluid inclusions were recorded using two instruments:1) on a Renishaw inVia spectrometer with StreamLineHR (Central Science Laboratory, University of Tasmania), using a 532-nm Nd:YAG laser with a power setting of 5 mW at the sampling spot, a 100x objective (0.85NA), a 1800 l/mm grating resulting in a spectral range of 115–1887 cm^{-1} and an acquisition time of 50 s. For 2D Raman maps, the following settings were employed: 532 nm laser with 12 mW at the sample spot, 50x objective (0.75NA), a 600 l/mm grating resulting in a spectral range of 100–4280 cm^{-1}, 0.1 s exposure time per pixel and a spatial resolution of 1x1 μm^2. 2D Raman map data were processed using an automated cosmic ray removal tool (Wire 5.2) and noise reduced using a principle component analysis. Colour images based on the different phases were created using the component analysis within Wire 5.2. 2) On a LabRAM HR800 dispersive Raman spectrometer (Institute of Geology and Mineralogy, Novosibirsk, Russia), using a 532-nm Nd:YAG laser with a power setting of 10 mW at the sampling spot, a 100x objective with a numerical aperture of 0.9 on a BX-51 microscope. The frequency was calibrated using the first-order Si line at 520.6 cm^{-1}. Spectra identification used the RRUFF database (https://rruff.info [University of Arizona, 2012]), as well as spectra reports by Arefiev et al. (2019) and Edwards et al. (2005).

5. Petrography

5.1. Ellendale 4

Sample E4 is a fragment of coherent (i.e. hypabyssal) lamproite derived from the 'central magmatic core' (see Jaques et al., 1986), which likely represents a former central lava lake. It contains abundant olivine (~30 vol%) occurring as large, rounded olivine macrocrysts (2–10 mm), as well as smaller euhedral (micro)phenocrysts (0.1–1 mm; Fig. 2a, b; Supplementary Fig. S1a). The majority of olivine grains are partially-to-completely replaced by pseudomorphs of serpentine and/or chlorite. Large (>5 mm) olivine macrocrysts are relatively well-preserved and only partially altered along rims and internal fractures, whereas smaller microcrysts (i.e. <~1mm) are usually completely altered. The groundmass is light-brown and very fine-grained (10–50 μm in size) and consists of (in order of relative abundance) euhedral phlogopite, apatite, perovskite, Cr-spinel (i.e. Ti-Al-Mg chromite – see Jaques, 2016; 15–30 μm in size), kinoshitalite ($(Ba,K)(Mg,Mn,Al)_3Si_2Al_2O_{10}(OH)_2$), along with abundant interstitial altered glass, chlorite and rare priderite [$(K,Ba)(Ti,Fe^{3+})_8O_{16}$; see also Jaques et al., 1986; Stachel et al., 1994]. Rare and thin (200 μm in thickness) veins of Ba-Sr-rich apatite aggregates traverse the groundmass. Based on the observed mineralogy, sample E4 is classified as a phlogopite-olivine lamproite.

5.2. Ellendale 9

Sample E9 is fragment of hypabyssal lamproite derived from the central core (i.e. former lava lake) of the E9 lamproite (see Jaques et al., 1986). It has macrocrystic texture with abundant (25–30 vol%) well-preserved olivine, which occurs as sporadic angular-to-rounded macrocrysts (1–10 mm in size) and abundant small euhedral (micro)phenocrysts (<1 mm in size; Fig. 2c, d; Supplementary Fig. S1b). Olivine exhibits minor alteration along rims and internal fractures, where it is partially replaced by serpentine. The groundmass is dark-brown and consists of (in order of relative

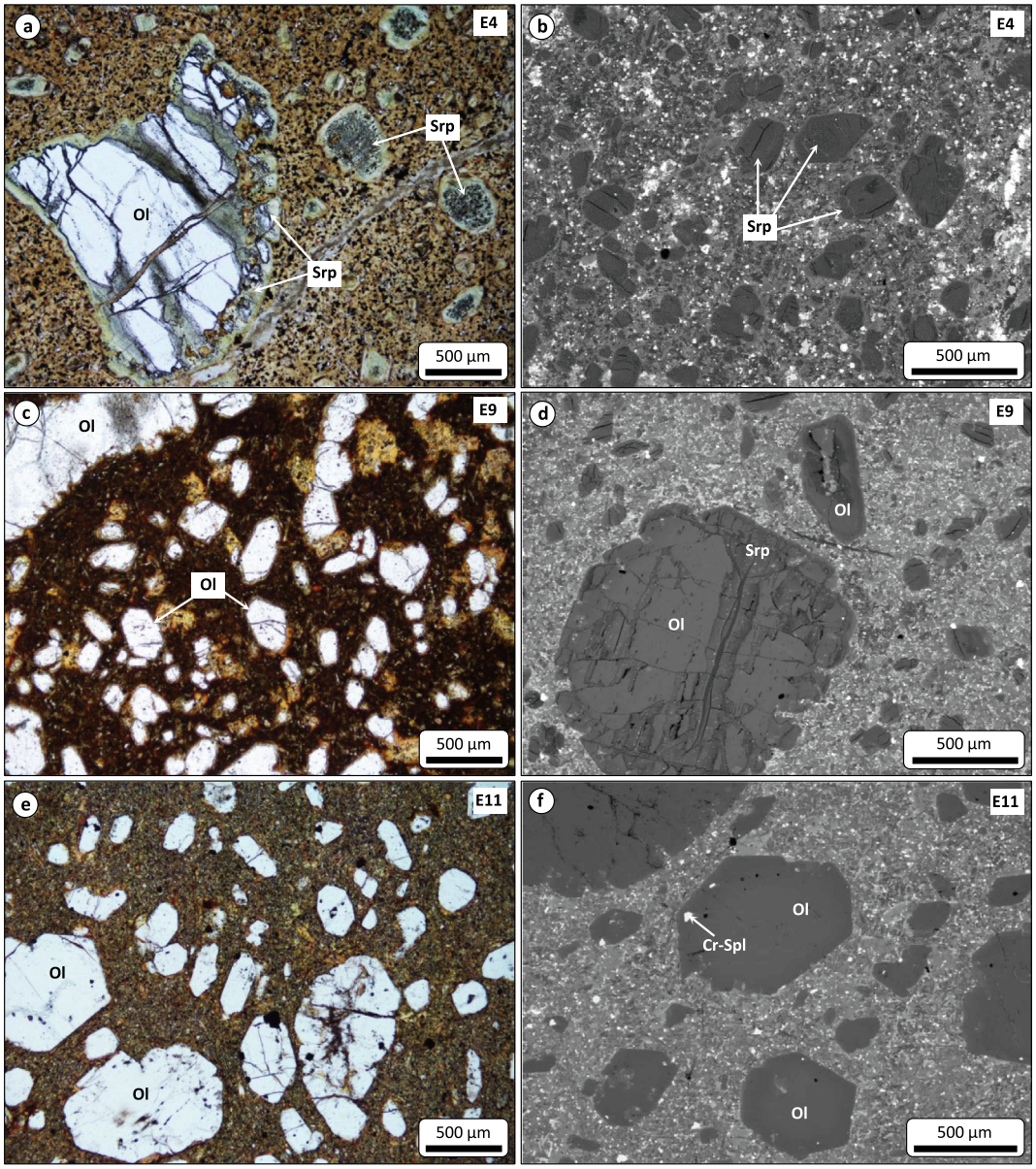

Fig. 2. Optical transmitted light (a, c, e) and back-scattered electron (BSE) SEM (b, d, f) images of the groundmass textures of the Ellendale lamproites: (a, b) E4, (c, d) E9, and (e, f) E11. Ol: olivine, Srp: serpentine, Cr-Spl: Cr-spinel.

abundance) abundant elongated euhedral grains of diopside (10–100 μm) and phlogopite (50–400 μm) along with lesser amounts of fine-grained (<30 μm) apatite, euhedral perovskite (5–20 μm in size) and Cr-spinel (e.g., Ti-Al-Mg chromite that is zoned towards more Fe-Ti-rich and Cr-poor rims; 20–80 μm in size), and rare wadeite and interstitial fresnoite ($Ba_2TiSi_2O_8$; see also Jaques et al., 1986; Stachel et al., 1994). Phlogopite forms large euhedral-shaped grains (up to several hundred μm in length and width) that contain euhedral inclusions of oxides (Cr-spinel, perovskite) and clinopyroxene, and are interstitial to olivine grains. The mesostasis assemblage is composed of interstitial glass, which is partially altered to chlorite. Based on the observed mineralogy, sample E9 is classified as a diopside-phlogopite-olivine lamproite.

5.3. Ellendale 11

Sample E11 is a fragment of hypabyssal lamproite derived from a former lava lake from the E11 lamproite vent (see Jaques et al., 1986). It has macrocrystic texture, which is defined by very abundant (~30 vol%) olivine, which occurs as subrounded-to-rounded macrocrysts (1–5 mm) and smaller euhedral (micro)phenocrysts (0.1–1 mm; Fig. 2e, f; Supplementary Fig. S1c). Olivine is well-preserved and exhibits minor or negligible serpentinisation along rims or fractures. The groundmass is dark-brown and very fine-grained (10–100 μm grain sizes) and is composed of (in order of relative abundance) euhedral leucite, diopside, apatite, phlogopite, perovskite (5–20 μm in size) and Cr-rich spinel (e.g., Ti-Al-Mg chromite that is zoned towards Fe-Ti-rich and Cr-poor rims; 50–150 μm in size), along with rare priderite. Cr-spinel has well-developed euhedral shapes and most minerals, including some olivine grains, are interstitial to it. The mesostasis assemblage is composed moderate-to-well preserved glass. In addition, the groundmass contains rare clusters (up to 1 mm in size) that are composed almost entirely of subhedral-to-euhedral grains of kalsilite (50–200 μm in size) and fine-grained celsian ($BaAl_2Si_2O_8$; <50 μm in size; Supplementary Fig. S2). Based on the observed mineralogy, sample E11 is classified as an olivine lamproite.

6. Olivine petrography and chemistry

The majority of olivine grain cores are homogenous in composition and exhibit narrow inter-grain variation in terms of Forsterite (Fo) content [(Mg / Mg + Fe^{2+}) × 100 mol.%], ranging from Fo 89.3 to 93.2 (average of 91.5 mol.%; Fig. 3; Supplementary Table S2). Minor elements exhibit limited variability, with CaO (0.01–0.13 wt%) and MnO very low (0.08–0.15 wt%), coupled with moderately high NiO (0.32–0.52 wt%; Supplementary Table S2; Fig. 3). These compositions show close compositional overlap with olivine macrocryst and phenocrysts cores reported for West Kimberley lamproite olivine (Jaques and Foley, 2018).

Olivine phenocrysts sometimes exhibit weak and diffuse (i.e. gradational) core to rim zoning (Supplementary Fig. S3). In addition, some olivine microcrysts (i.e. several hundred μm in size) exhibit a thin (up to ~100 μm in thickness) reversely zoned rim (~Fo_{91} based on SEM-EDS analyses).

Both olivine macrocrysts and phenocrysts from the E9 and E11 lamproite occasionally exhibit irregularly shaped boundaries and/or embayments, which are infilled by groundmass minerals (Fig. 2; Supplementary Fig. S3). Surrounding these embayments, as well as individual melt/fluid inclusions within olivine, are distinct compositional zones (Fig. 4g, h; Supplementary Fig. S3). These zones usually radiate outwards from the embayment/inclusion and have often highly irregular-to-amoeboid shape, ranging in width from a few through to several tens of microns. These zones can also be significantly wider (tens of μm) surrounding one side of a melt/inclusion, or extremely thin or absent on another side. These zones are characterised by significantly lower Fo (85.1–90.4; average: 87.7, n = 30; Fig. 3; Supplementary Table S2) and NiO (0.16–0.39 wt%), but higher MnO (0.18–0.45 wt%) and CaO (0.18–0.58 wt%) compared to the host olivine (Fig. 3; Supplementary Table S2). The low-Fo olivine in these zones extends the compositional range of olivine previously reported from the West Kimberley lamproites (Jaques et al., 1986; Stachel et al., 1994; Jaques and Foley, 2018).

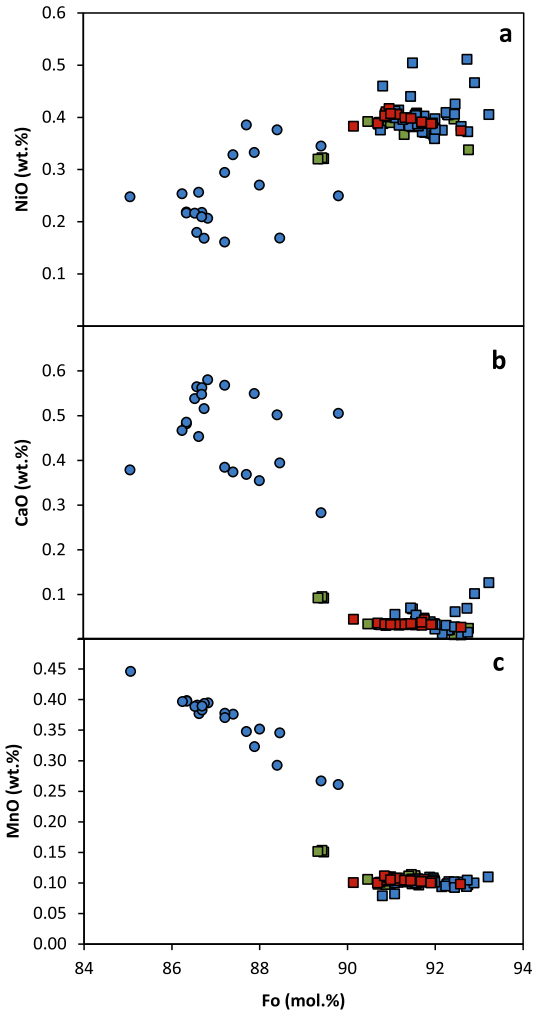

Fig. 3. Bivariate diagrams of Fo (mol.%) vs. (a) NiO, (b) CaO, and (c) MnO (wt.%) for olivine from the E4 (Green), E9 (Blue) and E11 (Red) lamproites. Squares denote the cores of olivine, whereas diamonds represent zoning (Z) surrounding inclusions in sample E9. (For interpretation of the references to colour in this figure legend, the reader is referred to the web version of this article.)

7. Inclusions

The compositions of inclusions in olivine, Cr-spinel and perovskite were examined by field emission SEM-EDS. Due to their small size, the quantification of individual phases in the inclusions was not undertaken by EMP. In addition, subsurface melt/fluid inclusions in olivine were examined by Raman spectroscopy.

7.1. Olivine

Three types of inclusions were identified in olivine: crystal, fluid and melt.

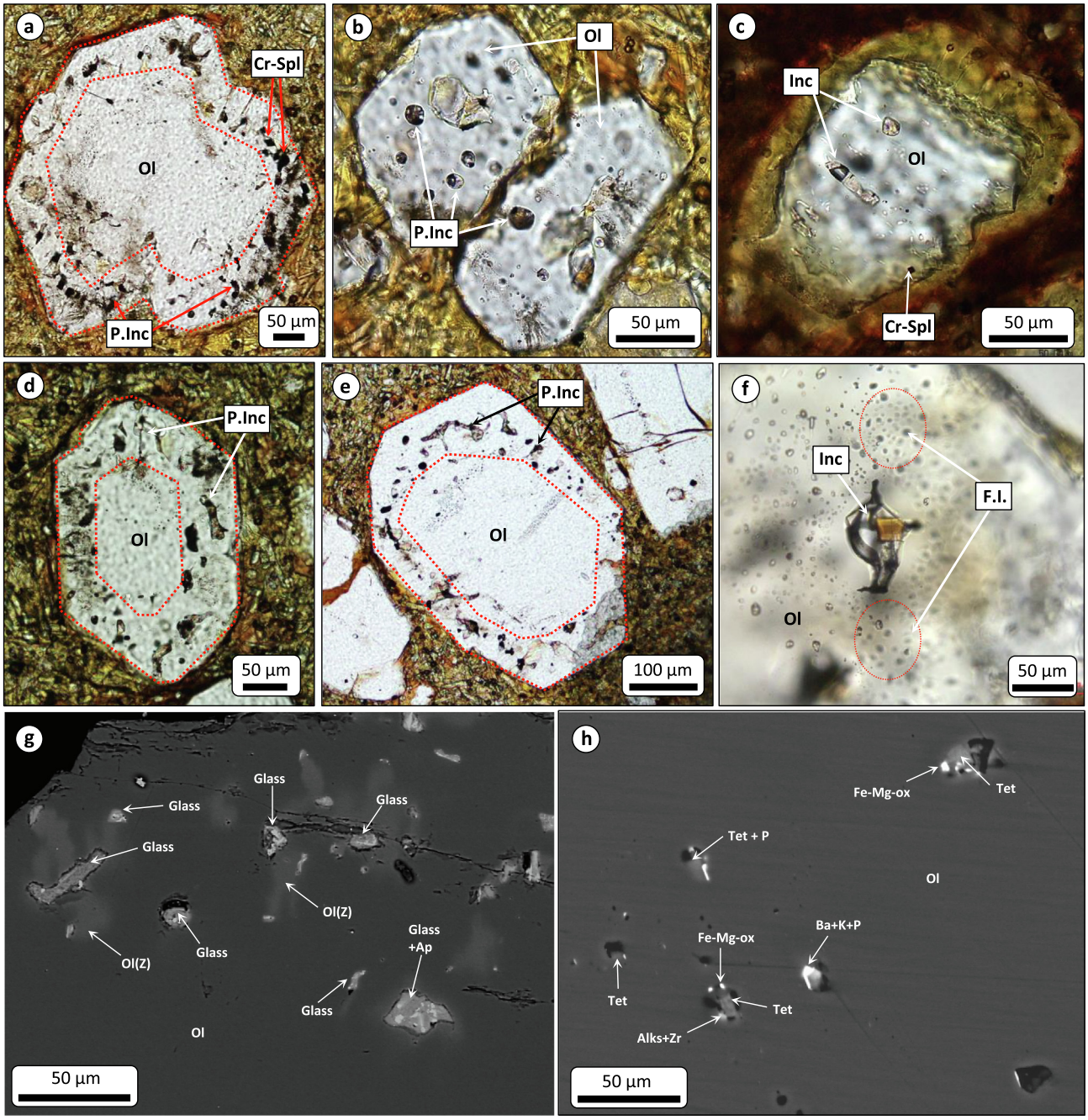

Fig. 4. (a–f) Optical transmitted light images showing the distribution of inclusions (Inc) in olivine (Ol). Primary inclusion (P.Inc) trails are distributed along the rims of euhedral olivine phenocrysts (a, d, e) or randomly distributed throughout the crystal (b), whereas trails of inclusions or inclusions aligned along fracture planes are likely psuedosecondary or secondary in origin (c, f). (g, h) Back-scattered electron (BSE) images of exposed secondary melt inclusion trails in olivine (Ol). (g) Melt inclusions in olivine are surrounded by irregular and patchy zoning (Ol(Z)), which is characterised by brighter, more Fe-rich compositions. Melt inclusions are commonly glass dominated, but may also contain daughter minerals. F.I.: fluid inclusions, Ap: apatite, Tet: tetraferriphlogopite, Alks: alkalis, Zr: zirconium, Ox: oxide.

Crystal inclusions comprise of rare euhedral Ti-Al-bearing magnesiochromite grains that range from 5 to 20 µm in size and are typically restricted to the rims of olivine phenocrysts (or their alteration products; see also Jaques, 2016; Jaques and Foley, 2018; Fig. 2f, 4a). These spinel inclusions in olivine are compositionally similar to the groundmass spinels and spinel inclusions in olivine previously reported in the Ellendale olivine lamproites (Jaques et al., 1986; Sobolev et al., 1989; Stachel et al., 1994; Jaques, 2016).

Fluid inclusions are very abundant (Fig. 4f) and are typically extremely small (1–5 µm in size), round-to-elongate in shape and transparent, where they form myriad clusters aligned along healed fracture planes that crosscut olivine macrocrysts and phenocrysts and are thus interpreted to be either as pseudosecondary (i.e. inclusions that formed along healed fractures during the growth of a crystal) or secondary in origin (see Roedder, 1984).

Melt inclusions are heterogeneously distributed in olivine grains, where they may be abundant in some grains, but absent in others. Melt inclusions are usually rounded-to-irregular in shape, range in size from < 5–20 µm (rarely up to 50 µm in size) and are multiphase, where they may consist of varying proportions of daughter minerals, glass and fluid (i.e. CO_2; Fig. 4b, c, f). Melt

inclusions typically occur as secondary/pseudosecondary trails along healed fractures in olivine macrocrysts and phenocrysts (Fig. 4b, c, f, g, h), but also as clusters of primary inclusions distributed along the margins of olivine phenocrysts (Fig. 4a, d, e).

The daughter mineral assemblages in olivine-hosted melt inclusions are heterogeneous, but show broad similarities in all three lamproites and consist of (in order of relative abundance) various Mg-Ca- (e.g., dolomite), Mg- (magnesite), K-Ca-Na-, K-Ca- [e.g., buetschliite ($K_2Ca(CO_3)_2$)], Na-H [e.g, nahcolite ($NaHCO_3$)], Ba- [witherite ($BaCO_3$)] bearing carbonates (additional unidentified carbonate minerals were also documented – see section of Raman spectroscopic study below), phosphates (e.g., fluorapatite and unidentified Na-Ba-bearing phosphates), perovskite and spinel of various compositions (e.g., Ti-Al-bearing magnesiochromite, as well as more evolved Mg-bearing magnetite and Fe-Ti-Mg-bearing spinel compositions), along with subordinate sylvite, K-Ba-bearing sulphates (arcanite– K_2SO_4, barite), F-bearing phlogopite, tetraferriphlogopite, Fe-Ni-Cu sulphides, haggertyite ($BaFe^{2+}_6Ti_5MgO_{19}$), wadeite ($K_2ZrSi_3O_9$), Mg-ilmenite, fresnoite ($Ba_2TiSi_2O_8$), noonkanbahite ($BaKNaTi_2(Si_4O_{12})O_2$), kalsilite, baddeleyite, enstatite, F-rich richterite ($K(NaCa)Mg_5Si_8O_{22}F_2$), diopside and pyrite; Fig. 4g, h, 5, 6; Supplementary Fig. S4 – 6; Table 2). In addition, some olivine macrocrysts in the E4 lamproite contain rare large (up to 300 μm) blebs and smaller (<5 μm) inclusion trails of Fe-Ni-Cu sulphides (including djerfisherite ($K_6Na(Fe^{2+},Cu,Ni)_{25}S_{26}Cl$)), which sometimes co-exist with the above mentioned melt/fluid inclusions (Supplementary Fig. S5). The glass component of the multi-phase inclusions varies depending on the size and proportion the mineral phases but can be 50% or more. Glass is characterized by high K, Ba, Mg (~11 MgO wt.% on average; based on SEM-EDS data), Ti contents and K/Na ratios, and low Al and Ca contents, which is broadly similar to leucite lamproite compositions (Jaques et al., 1986). In addition, carbonate contents vary from 12 to 32 vol%, sulphate, phosphate and chloride mineral content can reach up to 6 and 12 vol%, respectively, while silicate, titanate, sulphide and oxide mineral content can reach up to 5 and 10 vol%, respectively. A small number of inclusions were found to be dominated by uncommon daughter minerals, such as sylvite (e.g., Fig. 5f).

Raman spectroscopic study of daughter phases within inclusions.

According to our Raman spectroscopic study, melt/fluid inclusions in olivine contain a significant proportion of carbon compounds.

K-Na-Ca-carbonates were identified as the most common daughter mineral within inclusions (Fig. 7; Table 2; Supplementary Table S3). The general formula for this carbonate is $(K,Na)_2Ca(CO_3)_2$, however, the composition may vary from $K_{1.7}Na_{0.3}Ca(CO_3)_2$ to $K_{1.3}Na_{0.7}Ca(CO_3)_2$. To our knowledge, these are the first finds of carbonates in natural samples with a significant predominance of potassium over sodium in the cationic position A_2. In the $Na_2Ca(CO_3)_2$ – $K_2Ca(CO_3)_2$ series, carbonates were previously reported as Na-rich carbonates, including nyerereite (mineral with orthorhombic symmetry) and pure $K_2Ca(CO_3)_2$ carbonates, bütschliite (trigonal symmetry) and fairchildite (hexagonal symmetry) (e.g., Bolotina et al., 2017; Arefiev et al., 2019; Zucchini et al., 2022 and references therein). The mineral $(K,Na)_2Ca(CO_3)_2$ has one strong Raman band at 1089–1090 cm^{-1} and additional strong bands at 1079 and 1071 cm^{-1} (Fig. 7b), or a noticeable shoulder at 1073–1077 cm^{-1} (Supplementary Table S3). Additionally, several medium/weak Raman bands in the region 670–730 cm^{-1} ($\nu_4(CO_3)^{2-}$ vibrations; e.g., at 687, 704, 713 and 726 cm^{-1}; Fig. 7b) are present in the Raman spectra of this carbonate (Table 2; Supplementary Table S3). The Raman spectra of the $(K,Na)_2Ca(CO_3)_2$ carbonate is very different from those of bütschliite and fairchildite, but is similar to nyerereite in terms of shape (Golovin et al., 2017) with strongest band positions shifted to higher wavenumbers ~from 2 to 5 cm^{-1}. Thus, we assume that this carbonate can be considered as a potassium analogue of orthorhombic nyerereite and may be called K-nyerereite.

Bütschliite ($K_2Ca(CO_3)_2$) was identified by the following diagnostic Raman bands: a strong band at 1091 cm^{-1}, and six medium/weak bands at 67, 165, 222, 693, 1400 and 1765 cm^{-1} (Fig. 7c; Table 2; Supplementary Table S3; Arefiev et al., 2019).

Nahcolite ($NaHCO_3$) has the following diagnostic Raman bands: a strong band at 1046 cm^{-1}, and significant number medium/weak bands at 90, 112, 123, 143, 151, 164, 206, 226, 659, 686, 698, 1268,

Table 2
Raman band wavenumbers (cm^{-1}) of identified minerals among the daughter phases in the inclusions in olivine of West Kimberley lamproites.

Mineral	Olivine host	$(K,Na)_2Ca$-carbonate this study	Bütschliite	Nahcolite	Gregoryite/ Natrite	Magnesite	Norsethite	Alstonite	Unidentified phase this study	F-Apatite	Baddeleyite
Reference			(1)	(2)	(3)	(4)	(5)	(6)		(7)	(8)
Raman region (cm^{-1})											
0–500	223 m 303 m		67 m 165 m 222 m	90 m 112 m 123w 143 m 151w 164w 206w 226 m		209w 323 s	119 m 262w 299w		91w 124w 136w 149w 192 m	93 m 183 m 430 m 448w	**96 s** **175 s** **187 s** 218w 298w 332 m 343w 377w 472 m
501–1000	543 m 587 m 824 s 857 s 883 m 920 m 962 m	687w 704 m 713w 726w	693w	659w 686 m 698w	690 m 715 m 734w	738w	702w 882w	680w 697w 724w	573w 686w 697w 732w **984 s**	582w 590 m 606w **964 s**	502w 615w 635w
1001–2000		**1071 s** **1079 s** **1090 s**	**1091 s** 1400w 1765w	**1046 s** 1268 m 1436w 1623w	**1080 s**	**1094 s** 1758w	**1118 s** 1757w	**1066 s** 1090w 1758w	1045w **1060 s** 1387w 1464w 1738w	1041 m 1052 m 1080w	

Note: s = strong intensity, m = medium intensity, w = weak intensity.
References: (1) Arefiev et al., 2019; (2) Thomas et al., 2011 and RRUFF R070237; (3) Golovin et al., 2017; Buzgar and Apopei, 2009; (4) Perrin et al., 2016 and RRUFF R050676; (5) Böttcher et al., 1997; Schmidt et al., 2013; (6) Scheetz and White, 1977 and RRUFF R050483; (7) Antonakos et al., 2007 and RRUFF R050340; (8) Fukatsu et al., 2010 and RRUFF R060078.

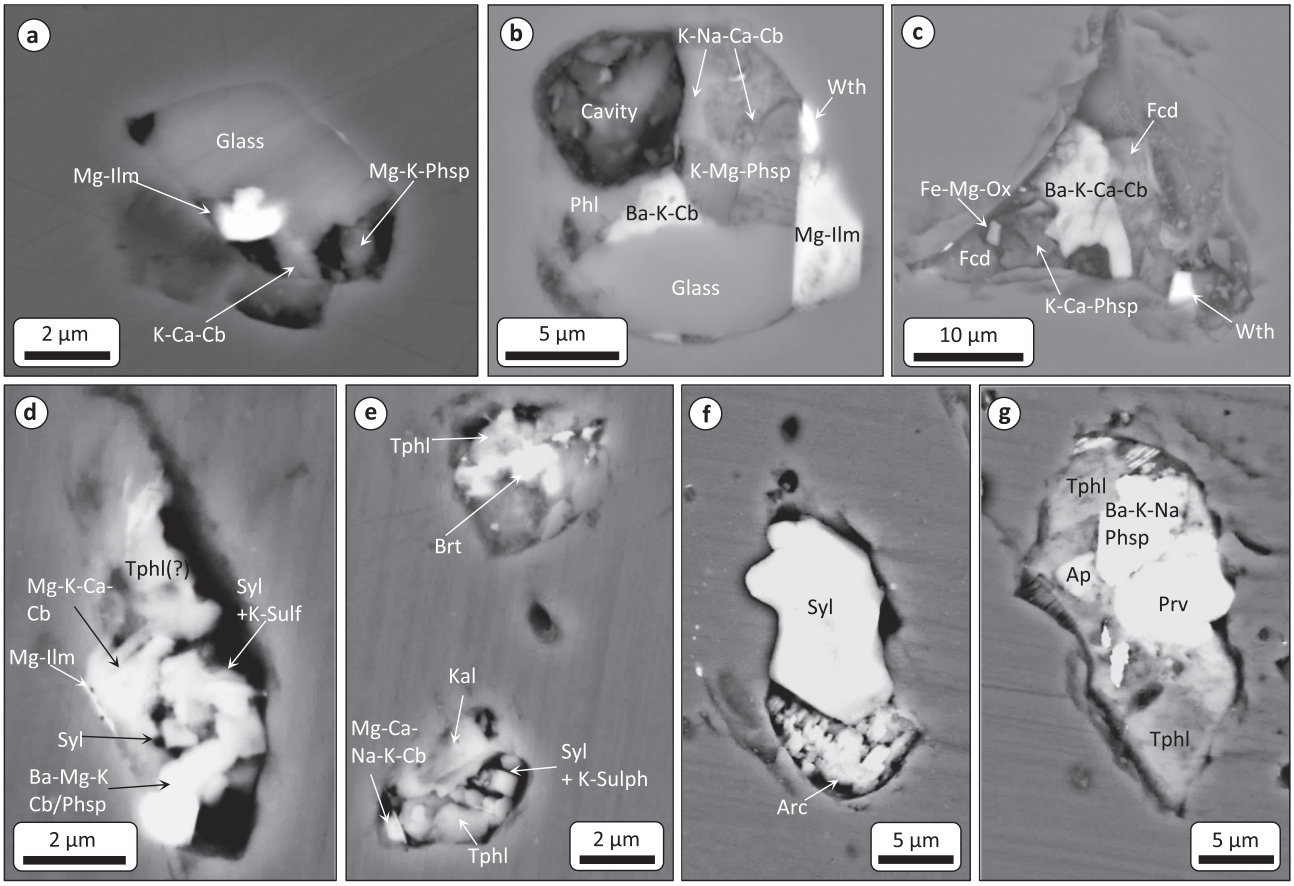

Fig. 5. (a–g) Back-scattered electron (BSE) images of exposed melt inclusions in olivine (Ol). Melt inclusions are typically composed of glass, as well as heterogeneous daughter assemblages of Mg-ilmenite (Ilm), phosphates (Phsp), carbonates (Cb), phlogopite (Phl), witherite (Wth), oxides (Ox), Fcd (fairchildite), tetraferriphlogopite (Tphl), sylvite (Syl), sulfates (Sulf), kalsilite (Kal), barite (Brt), arcanite (Arc), apatite (Ap), perovskite (Prv).

1436,1623 cm^{-1} (Fig. 7d; Table 2; Supplementary Table S3; Thomas et al., 2011; RRUFF database R070237).

The Raman spectra of gregoryite and natrite ($(Na,K,Ca)_2CO_3$/Na_2CO_3) are characterized by a strong band at 1080 cm^{-1} and weaker bands at 684 and 709 cm^{-1} (Fig. 7e; Table 2; Supplementary Table S3; Golovin et al., 2017; Buzgar and Apopei, 2009).

The following bands occur in the Raman spectrum of magnesite, $MgCO_3$: two strong bands at 323 and 1094 cm^{-1}, and three weak bands at 209, 738 and 1758 cm^{-1} (Fig. 7f, Table 2; Supplementary Table S3; Perrin et al., 2016; RRUFF database R050676).

The Raman spectrum of norsethite ($BaMg(CO_3)_2$) displays strong band at 1118 cm^{-1}, medium band at 119 cm^{-1} and weak bands at 262, 299, 702, 882, 1757 cm^{-1} (Fig. 7g, Table 2; Supplementary Table S3; Schmidt et al., 2013).

The Raman spectrum of alstonite ($BaCa(CO_3)_2$) are characterized by strong band at 1066 cm^{-1}, and weak bands at 680, 697, 724, 1090, 1758 cm^{-1} (Fig. 7h; Table 2; Supplementary Table S3; Scheetz and White, 1977; RRUFF database R050483).

In addition, the Raman spectroscopic study revealed the presence of the same phase(s) within the seven unexposed inclusions with Raman bands in the regions attributed to CO_3^{2-} and SO_4^{2-} or PO_4^{3-} main vibrations. We could not identify these phase(s) because of the lack of reference Raman spectra. The phase(s) have two strong bands in the regions 982–986 and 1059–1061 cm^{-1} in its Raman spectra (Supplementary Table S3), however, the Raman intensity of these bands relative to each other can differ significantly (Fig. 7i, j). Furthermore, these phase(s) are characterized by medium/weak bands at 91, 124, 136, 149, 192, 573, 686, 697, 732, 1045, 1387, 1464 and 1738 cm^{-1} (Fig. 7i, j). The strong Raman band at 1059–1061 cm^{-1} usually characterizes the main Raman vibrational mode CO_3^{2-} species, e.g., the strong band at 1062 cm^{-1} has the carbonate ion dissolved in H_2O and D_2O (Oliver and Davis, 1973) or the strong band at 1061 cm^{-1} has trona $Na_3(HCO_3)(CO_3)•H_2O$ (RRUFF database R050228) or the strong band at 1060 cm^{-1} is observed in Raman spectra K_2CO_3 or witherite $BaCO_3$ (Thomas et al., 2011; Buzgar and Apopei, 2009). The presence of CO_3^{2-} groups in these phase(s) are also confirmed by medium/weak Raman bands in the regions 680–740 and 1400–1800 cm^{-1} (Fig. 7i, j). The Raman bands in these regions are usually attributed to different vibrational modes of the CO_3^{2-} groups in various carbonates (e.g., Buzgar and Apopei, 2009; Frezzotti et al., 2012; Golovin et al., 2017). In addition, the strong Raman bands in the regions 982–986 and 1059–1061 cm^{-1} could be attributed to vibrational modes of the SO_4^{2-} groups. For example, eldfellite ($NaFe(SO_4)_{1.5}(X)_{0.5}$) has strong Raman band at 1060 cm^{-1} (Trussov et al., 2020) and langbeinite ($K_2Mg_2(SO_4)_3$) is characterized by a strong band at 1055 cm^{-1} (RRUFF database R070285).

Fluid inclusions or fluid bubbles within melt inclusions composed of carbon dioxide, which have the following diagnostic Raman bands: two strong band at 1285 and 1388 cm^{-1}, and additionally weak band at 1370 cm^{-1} (Fig. 8a; Supplementary Table S3; e.g., Frezzotti et al., 2012). Besides carbon dioxide, methane was identified in minor amounts in one fluid inclusion. Methane is characterized by the Raman band at 2917 cm^{-1} (Fig. 8b, Supplementary Table S3; Frezzotti et al., 2012).

7.2. Compositions of heated melt inclusions in olivine

The majority of olivine-hosted melt inclusions showed significant phase transformations on heating (heated to 1050 °C). These

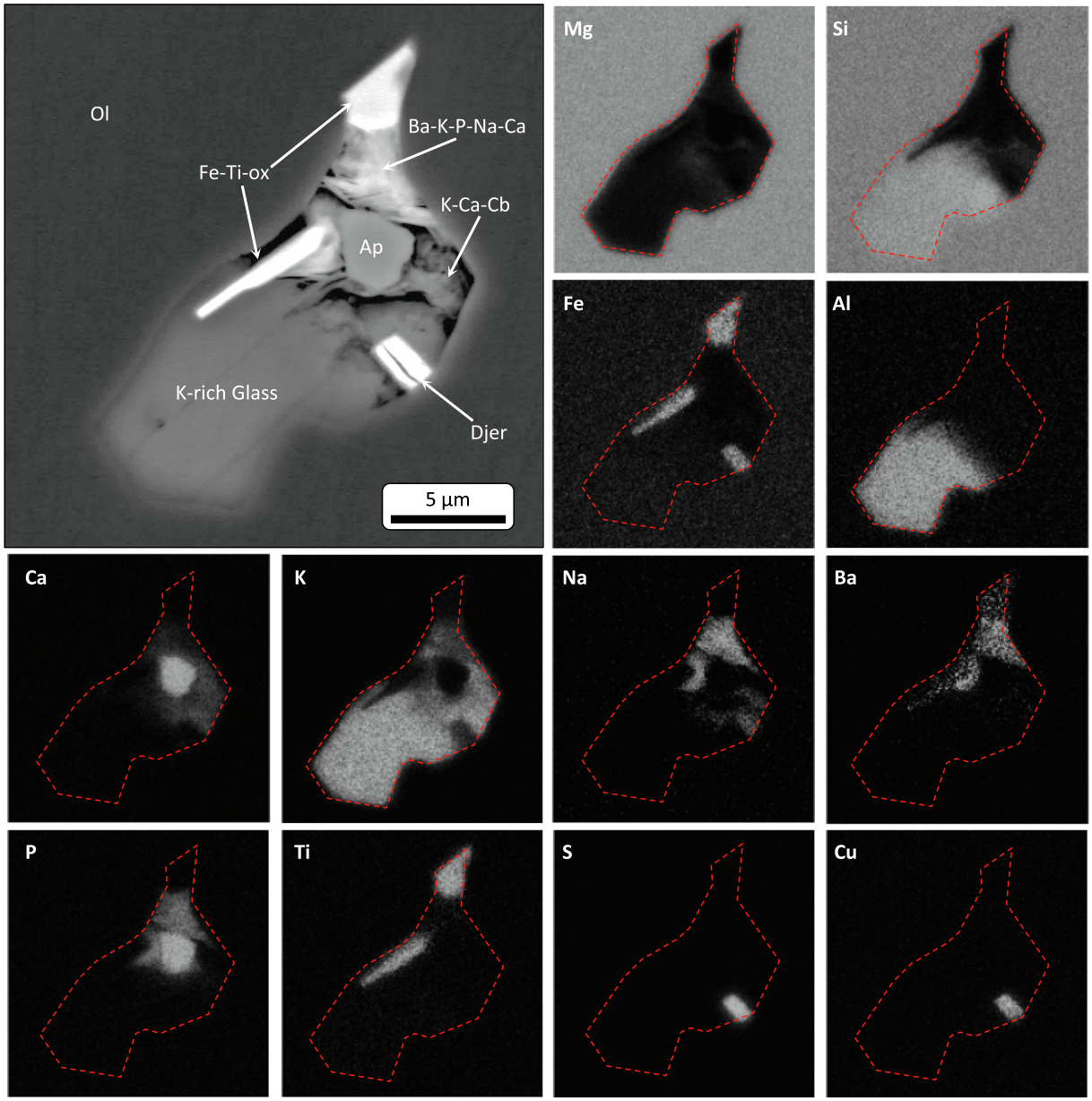

Fig. 6. Back-scattered electron (BSE) SEM image and X-ray element maps of a multiphase melt inclusion in olivine (Ol). The dotted red line shows the outline of the inclusion. Ap: apatite, Djer: djerfisherite, Ox: oxide, Cb: carbonate. In addition, the inclusion contains an unidentified Ba-K-P-Na-Ca-bearing daughter mineral. (For interpretation of the references to colour in this figure legend, the reader is referred to the web version of this article.)

inclusions are usually dominated by a light beige-brownish glass, the appearance of one or more distinct CO_2-rich shrinkage bubbles (Fig. 9a–c, 10; Supplementary Fig. S7) and the appearance of a clear immiscible component, which showed strong bands between 1076 and 1080 cm^{-1} and, to a lesser extent weak, bands between 984 and 985 cm^{-1}, indicating the presence of carbonate and sulphate, respectively (Supplementary Table S4).

The glass component in heated melt inclusions shows a close compositional overlap with heated glasses in melt inclusions previously reported for West Kimberley lamproites (Sobolev et al., 1989; Sharygin, 1991; Supplementary Table S5; Supplementary Fig. S8), but are generally richer in MgO, K_2O and in some rarer cases Al_2O_3. The presence of inclusion-hosted glasses in our study with MgO compositions anonymously high (>15 wt%) could be in part attributable to interference from the host olivine (i.e. secondary fluorescence). Crystalline daughter phases within heated melt inclusions are rare, small in size (<5 µm) and comprise of Fe-Mg-Cr oxides, perovskite and fluorapatite (Figs. 9, 10; Supplementary Fig. S7). Glasses in some inclusions are sometimes characterized by more than one composition (i.e. compositional variation in all major elements), indicating partial recrystallization or emulsion (Fig. 9d). In addition, a large proportion of Raman analyses of glasses showed the presence of a broad Raman band within the 1067 to 1080 cm^{-1} region, indicating the presence of an unidentified CO_3^{2-} component (e.g., emulsion of microscopic carbonate blebs) within the silicate glass (Fig. 9a–c; Supplementary Fig. S7; Supplementary Table S4).

7.3. Cr-spinel

Cr-spinel contains rare melt inclusions that are randomly distributed throughout the Cr-rich regions of the grain (i.e. never located along the more Fe-Ti-rich and Cr-poorer rims) and appear unrelated to any fracture system, and are thus interpreted to be

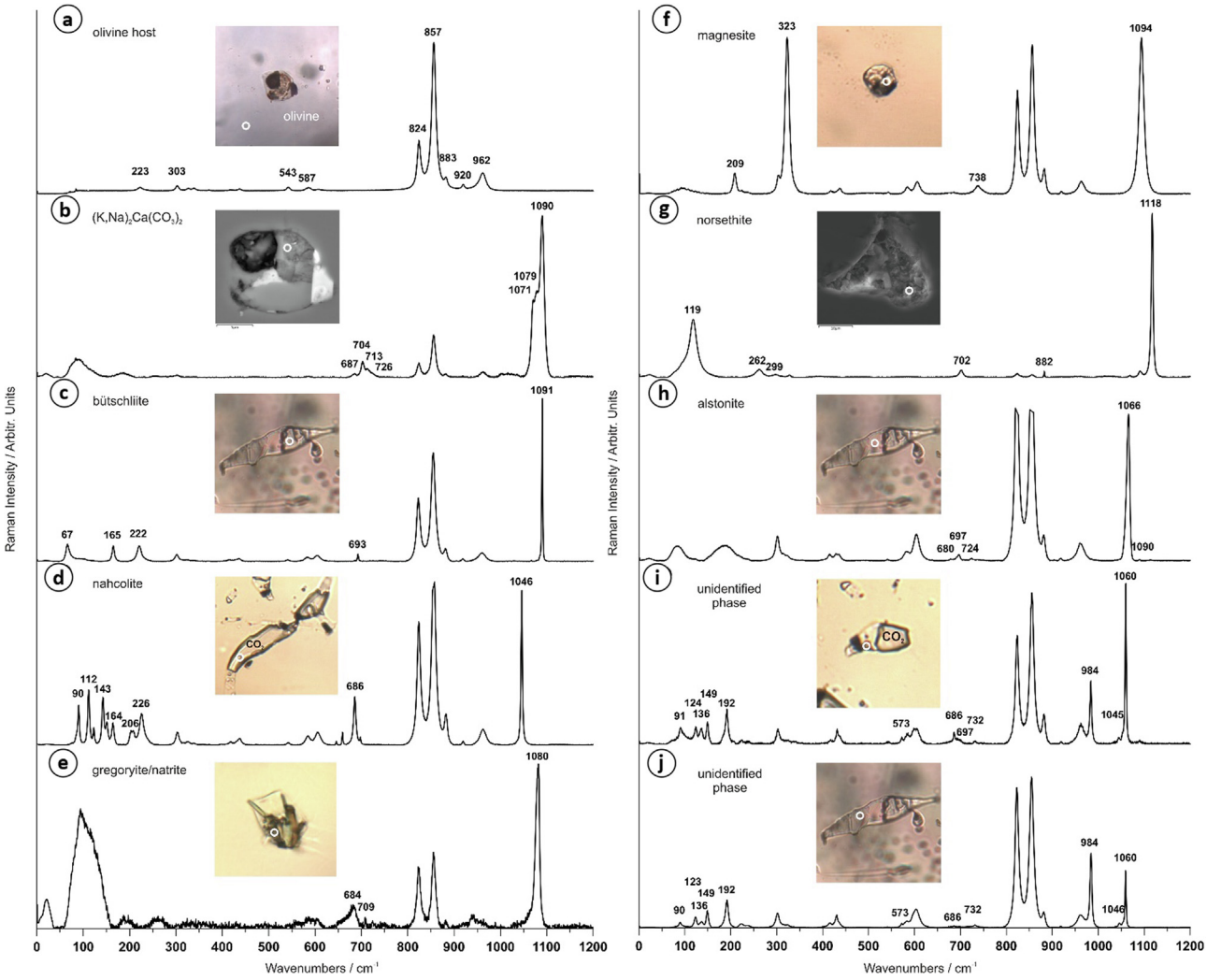

Fig. 7. Raman spectra of daughter carbonates within olivine-hosted exposed (b, g) and unexposed inclusions (c–f, h–j). Raman spectra of host olivine (a), $(K,Na)_2Ca(CO_3)_2$ carbonate (b), $K_2Ca(CO_3)_2$ bütschliite (c), $NaHCO_3$ nahcolite (d), $(Na_2,K_2,Ca)CO_3/Na_2CO_3$ gregoryite/natrite (e), $MgCO_3$ magnesite (f), $BaMg(CO_3)_2$ norsethite (g), $BaCa(CO_3)_2$ alstonite (h) and unidentified phase/phases (i, j) from olivine-hosted inclusions. Images (a, c–f, h–j) are in plane-polarized light and (b, g) are BSE-SEM images – image (b) is a BSE-SEM image of image (a). The Raman bands without number designation in panels (b) and (e) are Raman bands host olivine (see also panel a for comparison). Circles in the images indicate from where Raman spectra were collected.

primary in origin (Fig. 11). Melt inclusions in Cr-spinel are typically extremely small (2–15 μm), irregular in shape and comprise of (in order of relative abundance) glass (compositions analogous to glasses found in olivine-hosted melt inclusions), along with subordinate apatite and mixtures of unidentified K-Na-Ba-bearing carbonate and phosphate phases, phlogopite and diopside. In addition, Cr-spinel hosts rare crystal inclusions (<20 μm in size) of olivine (Fo_{89} based on SEM-EDS analyses).

7.4. Perovskite

Perovskite contains rare melt inclusions that are usually randomly distributed throughout the grain or aligned along growth zones and are thus likely primary in origin (Fig. 12). Melt inclusions are present in all parts of the perovskite grain, ranging from the core to exterior rim. These melt inclusions are usually small (1–5 μm in size) and round-to-elongate in shape. Due to their extremely small sizes, the composition of the daughter phases has to be considered only as qualitative. In general, daughter minerals included an unidentified Si-Mg-Ca-bearing phase (due to Ca interference from perovskite, this phase could be either olivine or clinopyroxene), apatite and alkali (Na, K) rich silicate glass (Fig. 12).

8. Discussion

8.1. Paragenetic sequence of Ellendale lamproites

The petrographic relationships and the relative sequence of included minerals in the zoned coarse-grained to pegmatitic Walgidee Hills lamproite suggests the paragenetic sequence for the major and minor crystallising silicate and titanate phases in the West Kimberley lamproites was likely olivine – Cr-spinel – diopside – perovskite – leucite – phlogopite – apatite – wadeite – priderite – ilmenite – titanian potassium richterite – sanidine – jeppeite – noonkanbahite (Jaques, 2017). Haggertyite occurs in the evolved groundmass a few olivine lamproites where it may take the place of or in some cases co-exist with ilmenite (Jaques et al., 2020). It is noteworthy that the presence of haggertyite in olivine-hosted melt inclusions in our samples provides additional support for the magmatic origin of this mineral in lamproites (Jaques et al., 2020). Phlogopite occurs as both microphenocrysts

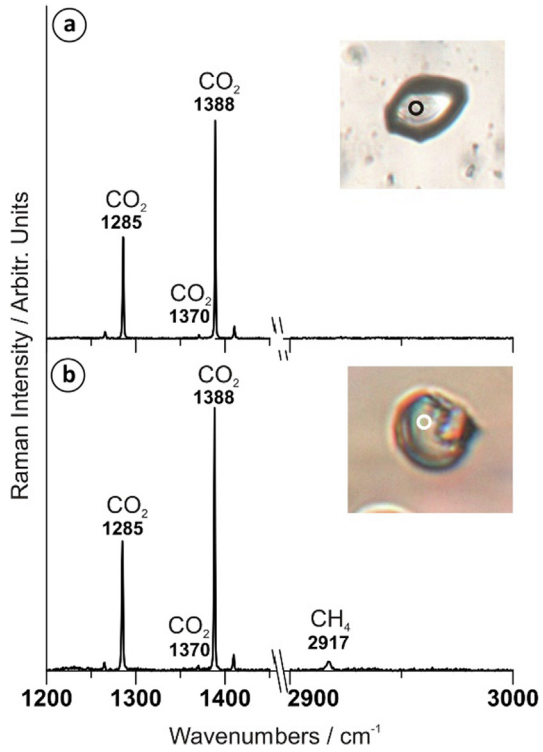

Fig. 8. Raman spectra of volatile compounds within inclusions. Raman spectra of carbon dioxide (a) and carbon dioxide with methane admixture (b) from olivine-hosted fluid/melt inclusions. (a, b) – unexposed inclusions, plane-polarized light.

which are commonly either free of or contain only a few inclusions, and as later crystallising more evolved mica forming poikilitic plates in the groundmass which commonly contain abundant inclusions Cr-spinel, perovskite, diopside, leucite, apatite, priderite, and wadeite (Jaques et al., 1984a, 1986). Barite is also a rare inclusion in phlogopite. This suggests either two generations of phlogopite or protracted crystallisation of phlogopite overlapping with that of apatite, priderite, and wadeite. The West Kimberley lamproites have low abundances of sulphur (Jaques et al., 1986) and contain only rare traces of sulphide minerals.

8.2. Timing of melt/fluid inclusion entrapment in olivine, Cr-spinel and perovskite

Olivine and Cr-spinel are commonly considered to be early crystallising minerals in mantle-derived magmas, such as kimberlites and lamproites (Sharygin et al., 1998; Fedortchouk and Canil, 2004; Foley et al., 2013). This is evident in our samples, where Cr-spinel occurs as euhedral crystal inclusions in the rims of olivine phenocrysts and the interstitial habit of other groundmass minerals surrounding olivine and Cr-spinel grains (e.g., Fig. 2f, 4a). Therefore, the entrapment of primary melt inclusion assemblages within olivine and Cr-spinel may represent snapshots of the early stage and subsequent stages of melt differentiation. Experiments have shown that the olivine stability field expands at low pressure in lamproite melts (e.g., Barton and Hamilton, 1978; Foley, 1989) and, together with olivine-spinel geothermometry, indicate that both olivine and Cr-spinel crystallized over an extended temperature interval (e.g., ~1220–850 °C; Stachel et al., 1994; Jaques, 2016). Perovskite occurs as euhedral chadacryst inclusions within phlogopite oikocrysts indicating that it also began to crystallise during the early-to-intermediate stages of groundmass crystallisation.

Melt inclusions in olivine, Cr-spinel and perovskite commonly contain glass, along with daughter minerals that are typical of the lamproite groundmass (e.g., fluorapatite, perovskite, phlogopite, diopside, wadeite, Mg-ilmenite, Fe-Mg-Ti-Cr spinel). The presence of noonkanbahite, haggertyite, tetraferriphlogopite and K-richterite, which are minerals characteristic of evolved lamproites (Mitchell and Bergman, 1991; Jaques et al., 1986; Hogarth, 1997), in some olivine-hosted melt inclusions indicates that olivine also entrapped late-stage or differentiated melts/fluids, or these inclusions could be attributed to the multiple generations of melt/fluid entrapment (i.e. primary vs. secondary origin). Based on analyses by Raman spectroscopy, the dominant volatile species in olivine-hosted melt/fluid inclusions is CO_2, whereas H_2O is either rare or absent. Similar results from the Ellendale lamproites were reported previously by Sobolev et al. (1989) and Sharygin (1997) who also found N_2, CO, CH_4, H_2, H_2S, NH_3, NO and HF as minor components of the fluid. This finding appears to conflict with the inclusions of phlogopite in olivine and spinel, and the abundance of groundmass phlogopite, apatite, and K-richterite in more extensively crystallized lamproites. All these phases have exceptionally high F contents in hydroxyl site (Jaques et al., 1986) but nevertheless indicate the presence of some water in the lamproite melt·H_2O-liquid in gas bubbles were reported in silicate melt inclusions in phlogopite in Ellendale lamproites by Sharygin (1997).

Many melt/fluid inclusions in olivine, and to a lesser extent in Cr-spinel, commonly contain daughter alkali/alkali-earth (Mg-Ca-, Mg-, K-Ca-Na-, K-Ca-, Na-, K-, Ba-) carbonates, phosphates and chlorides. These daughter minerals have been shown to be dominant constituents in melt inclusions in kimberlite minerals (e.g., Kamenetsky et al. 2007, 2013; Abersteiner et al., 2017, 2019), however, the distinguishing feature in melt inclusions in lamproites is the presence of a silicate glass component. Despite the widespread occurrence of these alkali/alkali-earth bearing carbonates, phosphates and chlorides in the melt inclusions, these minerals are extremely rare or absent in the groundmass of the Ellendale lamproites (e.g., Jaques et al., 1986). Thus, the origin of these carbonate, sulphate and chloride daughter minerals in olivine-hosted, and to some extent Cr-spinel hosted, melt inclusions and their relationship to the lamproitic magma requires further explanation.

8.3. Melt inclusions and their implications for lamproite melt compositions

Unlike many other alkaline mantle-derived magmas (e.g., carbonatites, kimberlites, ultramafic lamprophyres), lamproites rarely contain primary carbonate minerals, and have been commonly inferred to originate from reduced mantle sources poor in CO_2 but rich in H_2O and F (Jaques et al., 1984a; Bergman, 1987; Foley et al., 1986; Mitchell and Bergman, 1991). Although carbonates have been documented in a wide variety of lamproite localities worldwide, their origin is often loosely assigned to different sources. For example, some 'carbonate-bearing' lamproites from the Kaapvaal craton (or 'orangeites'; cf. Pearson et al., 2019; Mitchell, 2020; Tappe et al., 2022) and Raniganj (India) contain groundmass calcite (Mitchell, 1995a, Mitchell and Fareeduddin, 2009). The Jumilla lamproite (Spain) contains late-crystallised aggregates and veins of groundmass apatite, haematite and carbonates (i.e. calcite, dolomite), which, based on Sr-C-O isotope systematics, were inferred to be of mixed magmatic and sedimentary origin (Venturelli et al., 1991, 1993). The tuffs of the Argyle lamproite (Western Australia) contain widespread Sr- and Ba-bearing carbonates mostly as sparry anhedral patches in the groundmass but some occur as globule-like features in the groundmass resembling immiscible carbonate liquids (Jaques et al., 1984a). A secondary origin associated with hydrothermal or late-stage

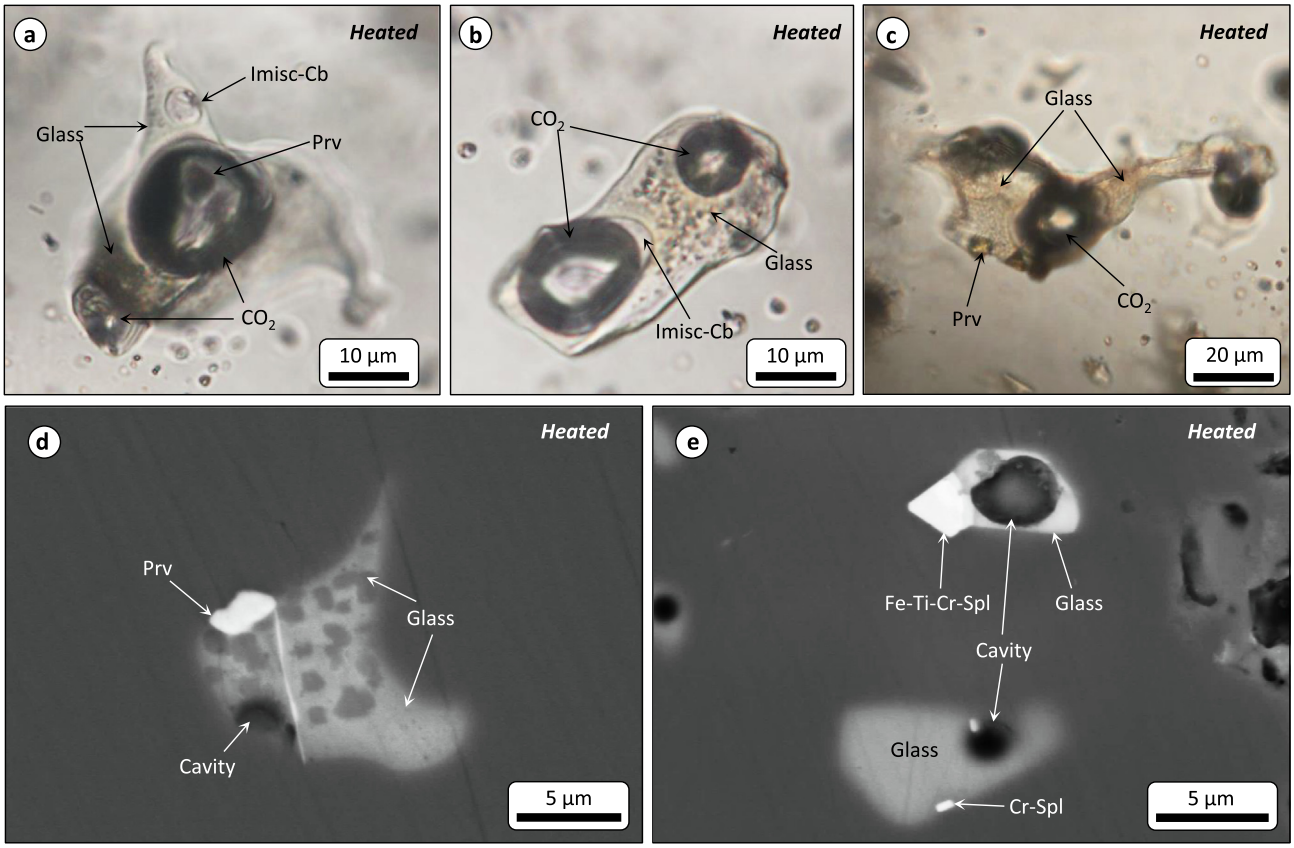

Fig. 9. (a–c) Optical transmitted light images of heated melt inclusion trails in olivine (Ol), where they typically contain glass, shrinkage bubbles (CO_2), immiscible carbonate globule (Imisc-Cb), carbonate (Cb) and daughter minerals (e.g., perovskite: Prv). (d, e) Back-scattered electron (BSE) SEM images of exposed heated melt inclusions in olivine. Exposed inclusions commonly contain cavities, which likely represent an escaped fluid phase. (d) Glasses show two different compositions, which is indicated by differences in contrast in BSE imaging and variations in all major elements. Spl: spinel.

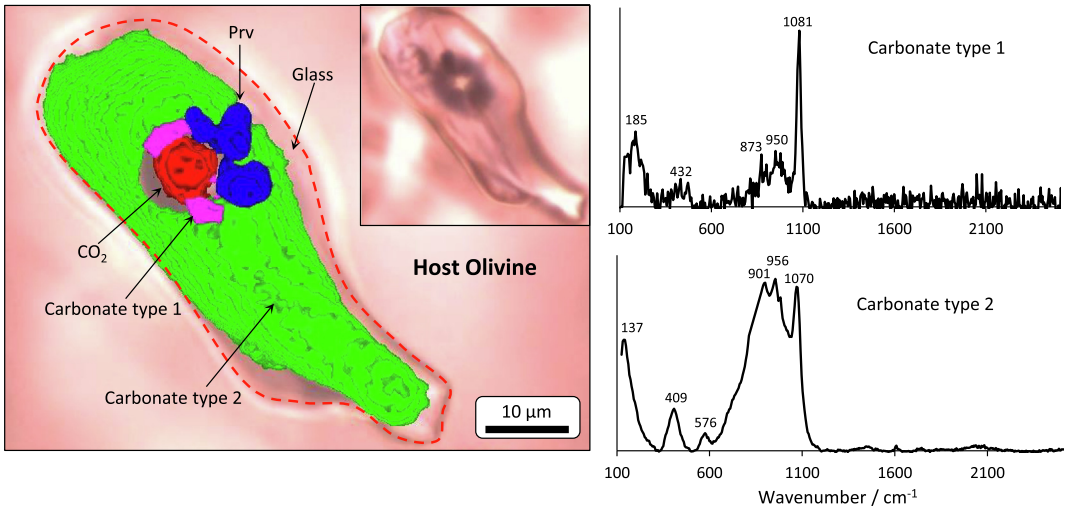

Fig. 10. Transmitted light optical image, false-colour 2D Raman map overlay, and representative Raman spectra of carbonate phases in a heated and unexposed melt inclusion in olivine. Phases identified include: carbonate, glass, perovskite and CO_2.

deuteric alteration is suggested by the $\delta^{18}O$-enriched composition of the vein-forming carbonate. Similarly, in the case of the Walgidee Hills lamproite (Western Australia), calcite veins located within the centre of the intrusion are interpreted to be the result of late-stage carbonate-rich deuteric or hydrothermal alteration (Jaques et al., 2020). Carbonate is also present in the Sisimiut (Greenland; Thy et al., 1987; Larsen and Rex, 1992) and Aillik Bay (Canada; Tappe et al., 2007) lamproites, which are located on opposite sides of the Labrador Sea from each other. The $\delta^{13}C$ composition of carbonates in Aillik Bay lamproites show that they range from −6.4 to −5.5 ‰, indicating a mantle origin (Tappe et al., 2007).

The widespread occurrence of carbonates in olivine-hosted melt inclusions is unexpected, as primary magmatic carbonates have

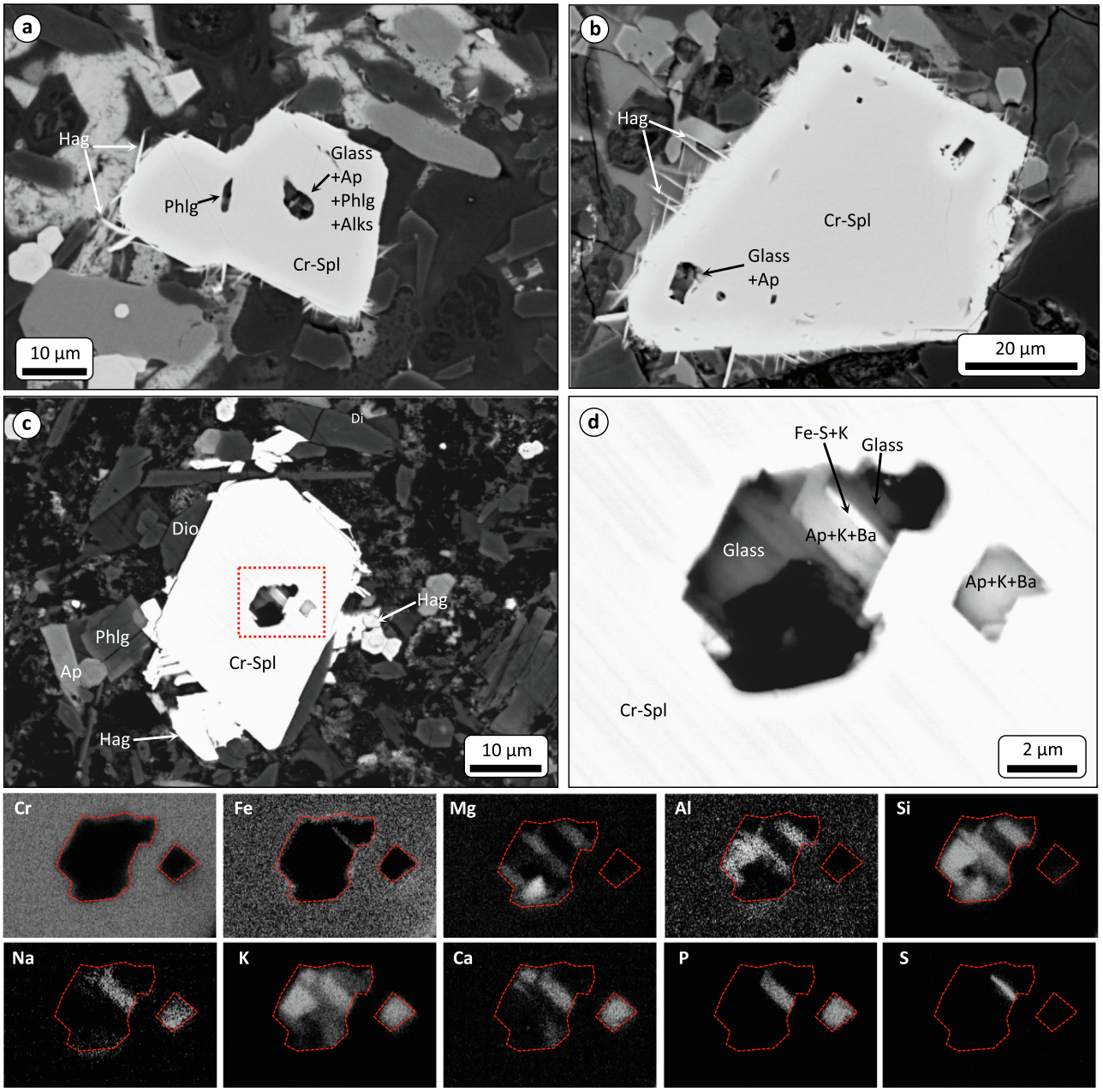

Fig. 11. (a–d) Back-scattered electron (BSE) SEM images of Cr-spinel (Spl) containing primary melt inclusions. Cr-spinel grains are commonly surrounded by radiating needles of haggertyite (Hag). Image (d) shows close up image of Cr-spinel-hosted inclusions in image panel (c) with corresponding X-ray element maps. The dotted red line shows the outline of the inclusions. Phlg: phlogopite, Gl: glass, Ap: apatite, Alks: alkalis, Sil: unidentified Si-phase. Dio: diopside, Kal: kalsilite. (For interpretation of the references to colour in this figure legend, the reader is referred to the web version of this article.)

not been found the groundmass of West Kimberley lamproites (Jaques et al., 1986). Average (n = 17) whole-rock analyses of the E4, E9 and E11 lamproites show that CO_2 contents are very low (~0.3 wt%) apart from one anomalous sample which contains 3.2 wt% CO_2 (Jaques et al., 1986). Although no detailed studies devoted to identify the origin or distribution of carbonates in these localities have been yet proposed, the majority of carbonates identified here have been assigned in literature either a secondary (e.g., hydrothermal or deuteric) origin. For example, Ellendale 4 is in close proximity to Devonian Reef complexes and may have inherited carbonate country rocks (Jaques et al., 1986). Similarly, the West Kimberley lamproites also exhibit low abundances of sulphur (Jaques et al., 1986) which, together with the rare traces of sulphide minerals in the groundmass, suggests S undersaturation throughout most of their crystallisation history.

Our study of different generations of melt (i.e. primary, pseudosecondary, secondary) inclusions in olivine and Cr-spinel from the E4, E9 and E11 olivine lamproites revealed that carbon, in the form of CO_3^{2-} and CO_2, was heterogeneously entrapped but was potentially an intrinsic part of the lamproitic magma. Heating experiments of melt/fluid inclusions in olivine revealed the presence of immiscible carbonate-rich sulphate-bearing globules (Figs. 9, 10; Supplementary Fig. S7), an exsolved CO_2 fluid (see also Sobolev et al., 1989; Sharygin, 1991, 1997), as well as dissolved carbonate (or micro-emulsion blebs) in the silicate glass (Supplementary Table S4). Analyses of daughter carbonates in melt inclusions show that they are enriched in alkalis/alkali-earths (K, Na, Ba,) and Mg, which reflects the high alkali and relatively low Ca content of the lamproite magmas. The widely differing proportions of silicate and carbonate components in these melt inclusions

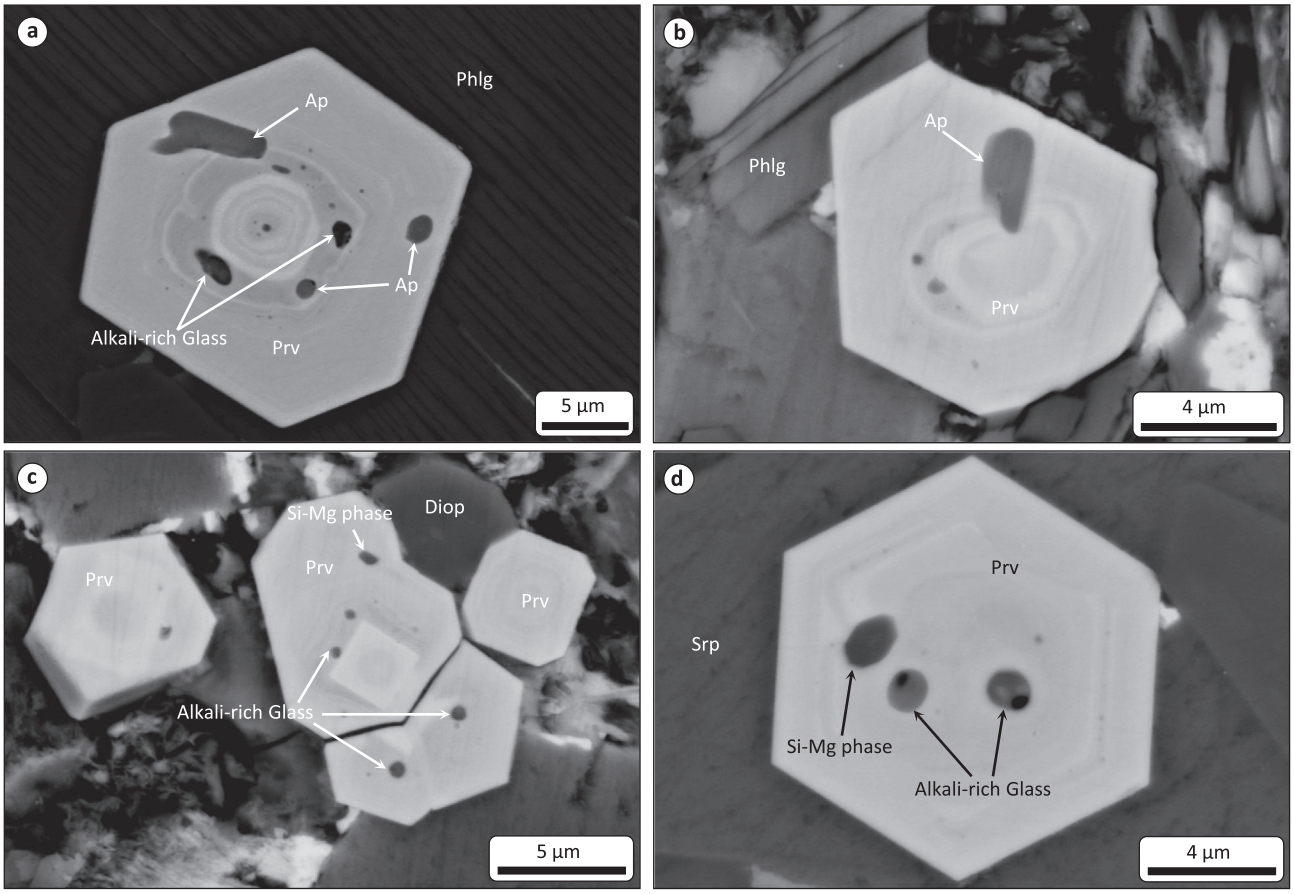

Fig. 12. Back-scattered electron (BSE) SEM images of groundmass perovskite (Prv). Perovskite is characterised by oscillatory zoning. Melt inclusions are randomly distributed throughout perovskite or aligned along growth zones. Some melt inclusions contain an unidentified Si-Mg phase. Ap: apatite, Phlg: phlogopite, Srp: serpentine.

likely reflects heterogeneous trapping of crystals and melt/fluid at various degrees of lamproite magma differentiation, and CO_2 and carbonate separation. The absence of carbonate, as well as sulphates and chlorides, in the lamproite groundmass could be due to a number of potential processes, including:

(1) The separation of an immiscible fraction (e.g., sulphate-carbonate-salt) from the dominantly silicate melt. This process can lead to the redistribution of elements, where Ca, alkalis/alkali-earths, CO_2, S, F, Cl, P and H_2O comprise the immiscible carbonate fraction, leaving the silicate melt poorer in these components and richer in Si (Panina and Motorina, 2008; Rokosova and Panina, 2013). This preferential partitioning of alkalis/alkali-earth and phosphorus into carbonate melts was demonstrated experimentally in both anhydrous and hydrous immiscible carbonate–silicate K-rich systems (Martin et al., 2013). Given the very small volume of carbonate-rich inclusions in olivine and absence of associated carbonatite magmas, this scenario is discounted as unlikely.

(2) Complete removal of carbonates, sulphates and chlorides from the groundmass during post-magmatic alteration or weathering. These minerals are highly soluble in water and susceptible to remobilization during post-magmatic alteration. This type of scenario was envisaged for kimberlitic (Abersteiner et al., 2018) and calciocarbonatitic (Zaitsev, 2010; Chen et al., 2013a) rocks, where alkali-carbonates and chlorides are abundant in melt inclusions hosted in a variety of xenocrystic and magmatic groundmass minerals but are absent in the host rock.

(3) Loss of CO_2 by degassing of the lamproite during eruption and crystallization as the solubility of CO_2 in magmas decreases markedly with decreasing pressure (Blank and Brooker, 1994; Dixon, 1997). Thus, during magma ascent (i.e. decompression) and eruption, the solubility of CO_2 will fall dramatically and CO_2 will be exsolved as a vapour potentially carrying other dissolved components such as K, Na, Ca, Ba, P, S, Cl and H_2O. Salvioli-Mariani et al. (2004) noted the presence of pure CO_2 bubbles in melt inclusions in olivine, leucite and clinopyroxene microphenocrysts from the Gaussberg lamproite (Antarctica) and suggested that CO_2 was exsolved at every stage of lamproite magma evolution whereas H_2O was retained in the melt during magma ascent and emplacement and largely quenched in the glassy groundmass (Salvioli-Mariani et al., 2004).

The discrepancy between the presence of carbonates and abundance of CO_2-rich melt/fluid inclusions in olivine and the lack of groundmass carbonate, the very low CO_2 contents in whole-rock analyses and the abundant hydrous phases (phlogopite and K-richterite) in the groundmass of the West Kimberley lamproites is similar to that observed in the Gaussberg lamproite which Salvioli-Mariana et al. (2004) attributed to the different behaviour of CO_2 and H_2O during crystallisation. The West Kimberley lamproites, like the Gaussberg lamproites, were erupted at low pressure with the volcanic craters of Ellendale pipes 4 and 9 infilled by lava lakes which are zoned from olivine lamproite at the margins to K-richterite-bearing phlogopite-olivine lamproite at the centre (Smith and Lorenz, 1989; Stachel et al, 1994). Decompression during ascent of the magma to the volcanic crater will cause

volatile exsolution (degassing) of the lamproite as solubility of both CO_2 and H_2O decrease with falling pressure. However, the partitioning of H_2O and CO_2 into the vapour phase during volatile exsolution will be controlled by the relative differences in their solubility with CO_2 more strongly partitioned into the vapour than H_2O, which will be retained longer in the melt (e.g., Dixon, 1997; Moussallam et al., 2016). The relative fractionation between CO_2 and H_2O will be less for lamproites and other alkaline rocks than tholeiitic basalts, where almost all the CO_2 may be lost before significant amounts of H_2O begin to exsolve, but will be enhanced by rapid decompression and under open system degassing where vapour is removed immediately upon exsolution (Dixon and Stolper, 1995; Dixon, 1997; Blundy and Cashman, 2008). Even under closed system degassing at low pressure, CO_2 will be preferentially exsolved and H_2O retained in the melt. Retention of H_2O in the melt is consistent with the increasing abundance of hydrous phases (phlogopite and K-richterite) in the more slowly cooled central parts of the lava lakes in Ellendale 4 and 9. Salvioli-Mariana et al. (2004) estimated, using the model of Stolper and Holloway (1988) and Pan et al. (1991) and the data of Thibault and Holloway (1994), the solubility of CO_2 in the Gaussberg lamproite at 1280 °C to be 0.23 wt% and 1.65 wt% at 1 kbar and 5 kbar, respectively.

Recently, experimental studies have modelled the solubilities of CO_2 and H_2O in putative SiO_2-poor kimberlite melts and have demonstrated that CO_2 solubility decreases with increasing SiO_2 content and the effect of pressure of CO_2 solubility is closely related to the SiO_2 content of the melt (Brooker et al., 2011; Moussallam et al., 2014; 2016). In contrast, H_2O solubilities in these speculated kimberlite melts is similar to that of common (e.g., basaltic) silicate melts. In contrast, the comparatively sparser availability of modern studies on the behaviour of CO_2 and H_2O in lamproite systems limits our ability to provide deeper and meaningful interpretations regarding the high H_2O/CO_2 of the Ellendale lamproites.

8.4. Formation of oxidised melts from reduced mantle

Experimental studies support an origin for the West Kimberley lamproites (and other lamproites generally; e.g., Barton and Hamilton, 1982; Mitchell and Bergman, 1991) by partial melting of strongly metasomatised lithospheric mantle (phlogopite-peridotite) under CO_2-poor, reducing and F-rich conditions with $H_2O > CH_4$ (Foley, 1985, 1989). In this reducing mantle melting scenario (with $fO_2 \sim$ iron-wüstite (IW) buffers ± 1–2 log units), carbon was likely initially present as CH_4 in the parental magma (Foley et al., 1986; Foley, 1993; Green, 2015). As the solubility of CH_4 is extremely low in these experimental peralkaline melts (up to 0.2 wt%; Foley, 1989), initial melts are likely to have had very low C contents and high H_2O/CO_2 ratios. Under more oxidized conditions, the mantle volatile species would be H_2O-CO_2 and partial melts would be increasingly silica-undersaturated (e.g., Foley and Pinter, 2018).

Early crystallised Cr-spinels in the Ellendale olivine lamproites indicate crystallisation under relatively reducing but more oxidising conditions than those suggested above for the mantle source region with fO_2 estimated from olivine-spinel oxygen barometry to be equivalent to the magnetite-wüstite (MW) buffer + 1–2 log units at ~1100–1250 °C (Foley, 1985; Stachel et al., 1994; Jaques, 2016). This indicates oxidation of the Ellendale olivine lamproite magmas during ascent from their mantle source. Foley et al. (1986) estimated that this could be achieved by dissociation of < 0.1 wt% H_2O through diffusive loss of H_2 from the magma. An additional mechanism proposed for inducing oxidation is via progressive degassing of the magma on ascent as carbon is dissolved in the melt as CO_3^{2-} and loss of volatiles on fluid saturation will increase the Fe_2O_3/FeO resulting in more oxidised conditions than the mantle source (Thibault and Holloway, 1994). Thus, an increase in fO_2 during magma ascent would also result in oxidation of CH_4 to CO_2. More recently, estimated redox equilibria from olivine-spinel pairs from the Kapamba lamproites (Luangwa Rift, Zambia) indicate they originated from a relatively oxidised source near the FMQ buffer (ΔFMQ + 1.7 ± 0.2 log units; Ngwenya and Tappe, 2021), similar to Aillikites and other craton and circumcratonic carbonate-bearing potassic magmatism. These lamproites are unusual as they contrast with the very-reduced and H_2O-F-rich conditions commonly inferred for the lamproite magma source (e.g., Foley et al., 1986), possibly owing to their more unique cratonic rift-related tectonic setting (Ngwenya and Tappe, 2021).

Increased fO_2 during low-pressure (i.e. crustal) crystallisation of the Ellendale lamproites is indicated by the abundance of carbonate and other oxidised species as inclusions. Late crystallising spinels in Ellendale 4 and 9 indicate crystallisation under significantly more oxidised conditions, with fO_2 increasing sharply to ~FMQ + 2–3 log units at 650–750 °C (Stachel and Brey 1993; Jaques, 2016).

The alkali-bearing (K > Na) carbonate, sulphate and chloride daughter assemblages found in olivine- and Cr-spinel-hosted melt/fluid inclusions bear similarities to the late-stage groundmass vein assemblages and associated apatite-hosted melt inclusions in the Jumilla lamproite (Venturelli et al., 1991, 1993), as well as olivine-hosted melt inclusions from the Smoky Butte lamproite (Sharygin et al., 1998). Similar daughter mineral assemblages are also common in magmatic- and xenocryst-hosted melt inclusions from other mantle-derived magmas, such as kimberlites (Kamenetsky et al., 2004, 2007; Abersteiner et al., 2017; Golovin et al., 2018) and carbonatites (Guzmics et al., 2011; Chen et al., 2013a; see also Supplementary Table S1), where, in the case of kimberlite rocks, the origin of these components is ascribed to the host melt at different stages of its evolution (i.e. early stages of differentiation in the mantle through to evolved late-stage melt after crustal emplacement). In the case of melt inclusions in our samples (olivine, Cr-spinel), the enrichment in alkali/alkali-earth carbonates may similarly be ascribed to be products of progressive melt enrichment in CO_2, alkali/alkali-earths, sulphur, phosphorus and halogens (Cl, F) in response to fractional crystallisation of silicate and oxide minerals (e.g., olivine, spinel, diopside) during the early stages of groundmass crystallisation.

Post-entrapment loss of water from melt/fluid inclusions can occur through rapid diffusion of H^+ and/or OH^- into the host olivine (Métrich and Wallace, 2008; Chen et al., 2011; Massare et al., 2002). Loss of water through diffusive re-equilibration from melt inclusions is enhanced at relatively high temperatures, and by slow cooling rates. Both these features apply to the Ellendale 4 and 9 pipes where the lamproites crystallized at high temperatures in lava lakes (Jaques et al., 1986; Smith and Lorenz, 1989; Stachel et al., 1994). The water concentration in melt inclusions in individual olivine hosts has been shown to correlate with the size (radius) of the melt inclusion, with the diffusive loss being greatest in smaller inclusions (Chen et al., 2013b). Diffusive water loss would, therefore, be enhanced by the small size of melt/fluid inclusions in the West Kimberley lamproites.

In summary, the distribution and role of carbon compounds (i.e. carbonates, CO_2) recorded in inclusions in the West Kimberley lamproites primarily reflects the different behaviour of CO_2 and H_2O on degassing of the magma during ascent, eruption and crystallisation. This has resulted in differences in mineralogy between the groundmass and melt/fluid inclusions hosted by phenocryst minerals. The Ellendale lamproites are inferred to have been derived from reduced mantle sources but the magmas became increasingly oxidised during magma ascent and crystallisation. The CO_2 and H_2O contents of the primary magma(s) are not well

constrained. The low CO_2 contents in the erupted magmas are minimum values after degassing and therefore were likely higher in the primary magma. This demonstrates the need for further investigations to assist in elucidating the original volatile inventory of lamproite magmas and how they are redistributed during magmatic ascent and upon emplacement. Moreover, certain aspects regarding the source of the carbonate and fluid components (e.g., mantle-derived and/or subduction-related) and their distribution within the West Kimberley and other lamproite provinces (e.g., orogenic vs. anorogenic) remains enigmatic. Further investigations of melt/fluid inclusions in carbonate-bearing lamproites (e.g., Raniganj, India; Sisimiut and Aillik Bay, Greenland/Canada) and orangeites (Kaapvaal craton, southern Africa), may provide further key insights into the origin and behaviour of volatiles (e.g., H_2O, CO_2) during lamproite petrogenesis and clarify potential petrogenetic links with or gradations towards other CO_2-riched magmas, such as orangeites, kamafugites, aillikites and specific types of ultramafic lamprophyres (Tappe et al., 2008).

9. Conclusions

- Melt/fluid inclusions in olivine, Cr-spinel and perovskite from three olivine lamproites (E4, E9 and E11) were studied and shown to contain daughter assemblages consisting of glass, along with abundant alkali/alkali-earth (Mg-Ca-, Mg-, K-Ca-Na-, K-Ca-, Na-, Ba-) carbonates, phosphates and chlorides, in addition to minerals (e.g., fluorapatite, perovskite, phlogopite, diopside, wadeite, Mg-ilmenite, Fe-Mg-Ti-Cr spinel) typical of the lamproite groundmass.
- The dominant volatile in melt/fluid inclusions in these Ellendale lamproites and other lamproites in general is CO_2, with H_2O being rare or absent.
- Although carbonates, sulphates and chlorides are common in melt/fluid inclusions in lamproite phenocrysts, these minerals are rare or absent from the host lamproite groundmass.
- The concentration of carbonate, along with alkalis/alkali-earths, halogens and sulphur observed in melt/fluid inclusions in minerals from the Ellendale lamproites resulted from progressive enrichment during crystallization and is associated with increasing oxidation of the lamproite magma. This appears to be a feature common to many lamproites.
- The presence of CO_2-rich, H_2O-poor fluid inclusions in the West Kimberley lamproites could be attributed to the preferential partitioning of CO_2 over H_2O into the vapour and retention of H_2O in the melt during volatile degassing rather than crystallization from magma derived from a mantle source with high CO_2/H_2O. Early partial degassing prior to entrapment of the inclusions is inferred to have been accentuated by post-entrapment loss of water through diffusion of H^+ and molecular H_2O from the very small inclusions.
- These features may be common to some other anorogenic lamproite provinces where inclusions in phenocrysts contain CO_2-rich inclusions but lack groundmass carbonate. Experimental studies indicate that lamproites and other related ultrapotassic rocks are typically derived from reduced lithospheric mantle sources. Their diverse compositions suggest formation at differing depths by partial melting of mantle with a range of volatile contents and oxygen fugacities.

CRediT authorship contribution statement

Adam Abersteiner: Conceptualization, Data curation, Investigation, Methodology, Project administration, Visualization, Writing. **Alexander Golovin:** Data curation, Formal analysis, Funding acquisition, Investigation, Writing, Formal analysis. **Ivan Chayka:** Writing, investigation. **Vadim S. Kamenetsky:** Funding acquisition, Dupervision, Writing. **Karsten Goemann:** Formal analysis, Data curation. **Thomas Rodemann:** Formal analysis, Data curation. **Kathy Ehrig:** Formal analysis, Data curationg.

Declaration of Competing Interest

The authors declare that they have no known competing financial interests or personal relationships that could have appeared to influence the work reported in this paper.

Acknowledgements

This study was jointly supported by the University of Tasmania, Australian Postgraduate Research (APR) Internship and the Institute of Volcanology and Seismology, RAS. AG and IC were supported by Russian Federation state assignment of IGM SB RAS. We would like to thank Lynton Jaques (Australian National University) for providing samples, the Fig. 1 map of Ellendale lamproites and invaluable discussions that greatly benefitted the development of this study. This manuscript benefitted from analytical assistance from M. Kamenetsky, discussions with V. Sharygin, and comments by Chris Clark, Aitor Cambeses, Stephen Foley, Bruce Kjarsgaard Dante Canil and two anonymous reviewers on earlier drafts of the paper.

Appendix A. Supplementary material

Supplementary Table 1. Optical transmitted light thin section scans of the E4, E9 and E11 lamproite samples. Ol: olivine. **Supplementary Figure 2.** (a – d) Back-scattered electron (BSE) SEM images of clusters of kalsilite (Kal) and celsian (Cel) grains intergrown in the E11 lamproite. Ol: olivine. **Supplementary Figure 3.** (a, b) Back-scattered electron (BSE) SEM images of olivine (Ol) from the E9 lamproite showing patchy Fe-rich zoning (Ol(Z) surrounding inclusions (Inc). **Supplementary Figure 4.** Back-scattered electron (BSE) SEM images and X-ray element maps of a multiphase melt inclusion in olivine (Ol). Two different composition glasses are present within the inclusion. Phlg: phlogopite, Ox: oxide, Cb: carbonate, S: sulphide. In addition, the inclusion contains unidentified K-Ca-P-Ba-rich daughter minerals. The dotted red line shows the outline of the inclusion. **Supplementary Figure 5.** Back-scattered electron (BSE) SEM images of (E4 lamproite): (a) sulphide-rich (S) globule composed of Fe-Ni-sulphides, Fe-Cu-sulphides, djerfisherite (Dj), wadeite (Wad) and an unidentified Fe-rich silicate (Sil) phase, and (b) trails of sulphides composed of Fe-Ni-Cu-sulphides and Ni-Fe-sulphides in olivine (Ol). Srp: serpentine. **Supplementary Figure 6.** (a – d) Representative Raman spectra of daughter (a – c) carbonates and (d) noonkahbahite in unheated multiphase inclusions in olivine. (e, f) Representative Raman spectra of carbonate globules in heated multiphase inclusions in olivine. **Supplementary Figure 7.** Optical transmitted light images of heated mutliphase melt/fluid inclusion trails. CO_2: bubble, Cb: carbonate, Pvk: perovskite, Mag: magnetite, Imisc-Cb: immiscible carbonate. **Supplementary Figure 8.** Bivariate plots of MgO (wt. %) vs. major element (wt.%) compositions for: i) heated glasses in olivine-hosted melt inclusions from the E4, E9 and E11 lamproites (this study; red squares – SEM-EDS data), ii) heated glasses in melt inclusions from phlogopite, apatite and olivine from Western Kimberley lamproites (Sharygin, 1991; blue squares – EMP data), and iii) heated glasses in melt inclusions from olivine and clinopyroxene from Western Kimberley lamproites (Sobolev et al., 1989; green squares – EMP data). Supplementary data to this article can be found online at https://doi.org/10.1016/j.gr.2022.06.005.

References

Abersteiner, A., Giuliani, A., Kamenetsky, V.S., Phillips, D., 2017. Petrographic and melt-inclusion constraints on the petrogenesis of a magmaclast from the Venetia kimberlite cluster, South Africa. Chem. Geol. 455, 331–341. https://doi.org/10.1016/j.chemgeo.2016.08.029.

Abersteiner, A., Kamenetsky, V.S., Golovin, A.V., Kamenetsky, M., Goemann, K., 2018. Was crustal contamination involved in the formation of the serpentine-free Udachnaya-East kimberlite? New insights into parental melts, liquidus assemblage and effects of alteration. J. Petrol. 59, 1467–1492. https://doi.org/10.1093/petrology/egy068.

Abersteiner, A., Kamenetsky, V.S., Goemann, K., Giuliani, A., Howarth, G.H., Castillo-Oliver, M., Thompson, J., Kamenetsky, M., Cherry, A., 2019. Composition and emplacement of the Benfontein kimberlite sill complex (Kimberley, South Africa): Textural, petrographic and melt inclusion constraints. Lithos 324–325, 297–314. https://doi.org/10.1016/j.lithos.2018.11.017.

Arefiev, A.V., Podborodnikov, I.V., Shatskiy, A.F., Litasov, K.D., 2019. Synthesis and Raman Spectra of K-Ca Double Carbonates: $K_2Ca(CO_3)_2$ Bütschliite, Fairchildite, and $K_2Ca_2(CO_3)_3$ at 1 Atm. Geochemistry International 57, 981–987. https://doi.org/10.1007/BF00376084.

Barton, M., Hamilton, D.L., 1982. Water-undersaturated melting experiments bearing upon the origin of potassium-rich magma. Mineral. Mag. 45, 267–278. https://doi.org/10.1180/minmag.1982.045.337.30.

Barton, M., Hamilton, 1978. Water-saturated melting relations to 5 kilobars of three Leucite Hills lavas. Contrib. Miner. Petrol. 66 (1), 41–49. https://doi.org/10.1007/BF00376084.

Bergman, S.C., 1987. Lamproites and other potassium-rich igneous rocks: a review of their occurrence, mineralogy and geochemistry. Geolog. Soc., London, Special Publ. 30 (1), 103–190. https://doi.org/10.1144/gsl.sp.1987.030.01.08.

Blank, J.G., Brooker, R.A., 1994. Experimental studies of Carbon Dioxide in silicate melts: Solubility, Speciation, and Stable Carbon Isotope behavior. In: Carroll, M. R., & Holloway, S.R. (Eds.), Volatiles in Magmas, Mineralogical Society of America 30, 157-186. https://doi.org/10.1515/9781501509674-011.

Blundy, J., Cashman, K., 2008. Petrologic reconstruction of magmatic system variables and processes. Rev. Mineral. Geochem. 69 (1), 179–239. https://doi.org/10.2138/rmg.2008.69.6.

Böttcher, M.E., Gehlken, P.L., Skogby, H., Reutel, C., 1997. The vibrational spectra of BaMg (CO3) 2 (norsethite). Mineralogical Magazine 61 (405), 249–256. https://doi.org/10.1180/minmag.1997.061.405.08.

Bolotina, N.B., Gavryushkin, P.N., Korsakov, A.V., Rashchenko, S.V., Seryotkin, Y.V., Golovin, A.V., Moine, B.N., Zaitsev, A.N., Litasov, K.D., 2017. Incommensurately modulated twin structure of nyerereite $Na_{1.64}K_{0.36}Ca(CO_3)_2$. Acta Cryst B73, 276–284. https://doi.org/10.1107/S2052520616020680.

Brooker, R., Sparks, R., Kavanagh, J., Field, M., 2011. The volatile content of hypabyssal kimberlite magmas: some constraints from experiments on natural rock compositions. Bull. Volcanol. 73 (8), 959–981 https://doi:10.1007/s00445-011-0523-7.

Buzgar, N., Apopei, A.I., 2009. The Raman study of certain carbonates. Geologie Tomul L 2 (2), 97–112.

Chayka, I.F., Sobolev, A.V., Izokh, A.E., Batanova, V.G., Krasheninnikov, S.P., Chervyakovskaya, M.V., Kontonikas-Charos, A., Kutyrev, A.V., Lobastov, B.M., Chervyakovskiy, V.S., 2020. Fingerprints of Kamafugite-Like Magmas in Mesozoic Lamproites of the Aldan Shield: Evidence from Olivine and Olivine-Hosted Inclusions. Minerals 10 (4), 337. https://doi.org/10.3390/min10040337.

Chen, W., Kamenetsky, V.S., Simonetti, A., 2013a. Evidence for the alkaline nature of parental carbonatite melts at Oka complex in Canada. Nat. Commun. 4, 2687. https://doi.org/10.1038/ncomms3687.

Chen, Y., Provost, A., Schiano, P., Cluzel, N., 2011. The rate of water loss from olivine-hosted melt inclusions. Contrib. Miner. Petrol. 162 (3), 625–636. https://doi.org/10.1007/s00410-011-0616-5.

Chen, Y., Provost, A., Schiamo, P., Cluze, N., 2013b. Magma ascent rate and initial water concentration inferred from diffusive water loss from olivine-hosted melt inclusions. Contrib. Miner. Petrol. 165, 525–541. https://doi.org/10.1007/s00410-012-0821-x.

Davies, G.R., Stolz, A.J., Mahotkin, I.L., Nowell, G.M., Pearson, D.G., 2006. Trace Element and Sr–Pb–Nd–Hf Isotope Evidence for Ancient, Fluid-Dominated Enrichment of the Source of Aldan Shield Lamproites. J. Petrol. 47 (6), 1119–1146. https://doi.org/10.1093/petrology/egl005.

Dawson, J.B., 1987. The kimberlite clan: relationship with olivine and leucite lamproites, and inferences for upper-mantle metasomatism. Geological Society, London, Special Publications 30, 95–101. https://doi.org/10.1144/GSL.SP.1987.030.01.07.

Dixon, J.E., 1997. Degassing of alkalic basalts. Amer. Mineral 82 (3-4), 368–378.

Dixon, J.E., Stolper, E.M., 1995. An experimental study of water and carbon dioxide solubilities in mid-ocean ridge basaltic liquids. Part II: applications to degassing. J. Petrol. 36 (6), 1633–1646. https://doi.org/10.1093/oxfordjournals.petrology.a037268.

Edwards, H.G., Villar, S.E.J., Jehlicka, J., Munshi, T., 2005. FT–Raman spectroscopic study of calcium-rich and magnesium-rich carbonate minerals. Spectrochim. Acta Part A Mol. Biomol. Spectrosc. 61 (10), 2273–2280. https://doi.org/10.1016/j.saa.2005.02.026.

Fedortchouk, Y., Canil, D., 2004. Intensive Variables in Kimberlite Magmas, Lac de Gras, Canada and Implications for Diamond Survival. J. Petrol. 45 (9), 1725–1745. https://doi.org/10.1093/petrology/egh031.

Foley, S.F., 1985. The oxidation state of lamproitic magmasDer Oxidationsgrad lamproitischer Magmen. Tschermaks Petr. Mitt. 34 (3-4), 217–238.

Foley, S.F., 1989. Experimental constraints on phlogopite chemistry in lamproites: 1. The effect of water activity and oxygen fugacity. Eur. J. Mineral. 1 (3), 411–426. https://doi.org/10.1127/ejm/1/3/0411.

Foley, S.F., 1992. Vein-plus-wall-rock melting mechanisms in the lithosphere and the origin of potassic alkaline magmas. Lithos 28 (3–6), 435–453. https://doi.org/10.1016/0024-4937(92)90018-T.

Foley, S.F., 1993. An experimental study of olivine lamproite: First results from the diamond stability field. Geochim. Cosmochim. Acta 57 (2), 483–489. https://doi.org/10.1016/0016-7037(93)90448-6.

Foley, S.F., Pintér, Z., 2018. Primary melt compositions in the Earth's mantle. Magmas Under Pressure, Elsevier: 3-42. https://doi.org/10.1016/B978-0-12-811301-1.00001-0.

Foley, S.F., Taylor, W.R., Green, D.H., 1986. The role of fluorine and oxygen fugacity in the genesis of the ultrapotassic rocks. Contr. Mineral Petrol. 94, 183–192. https://doi.org/10.1007/BF00592935.

Foley, S.F., Venturelli, G., Green, D.H., Toscani, L., 1987. The ultrapotassic rocks: characteristics, classification, and constraints for petrogenetic models. Earth Sci. Rev. 24, 81–134. https://doi.org/10.1016/0012-8252(87)90001-8.

Foley, S.F., Prelevic, D., Rehfeldt, T., Jacob, D.E., 2013. Minor and trace elements in olivines as probes into early igneous and mantle melting processes. Earth Planet. Sci. Lett. 363, 181–191. https://doi.org/10.1016/j.epsl.2012.11.025.

Frezzotti, M.L., Tecce, F., Casagli, A., 2012. Raman spectroscopy for fluid inclusion analysis. J. Geochem. Explor. 112, 1–20. https://doi.org/10.1016/j.gexplo.2011.09.009.

Fukatsu, K., Zhu, W., Pezzotti, G., 2010. Raman tensor analysis of baddeleyite single-crystal and its application to define crystallographic domains in polycrystalline zirconia. physica status solidi (b) 247 (2), 278–287. https://doi.org/10.1002/pssb.200945358.

Golovin, A.V., Korsakov, A.V., Gavryushkin, P.N., Zaitsev, A.N., Thomas, V.G., Moine, B.N., 2017. Raman spectra of nyerereite, gregoryite and synthetic pure Na2Ca (CO3)2: diversity and application for the study micro inclusions. J. Raman Spectrosc. 48, 1559–1565. https://doi.org/10.1002/jrs.5143.

Golovin, A.V., Sharygin, I.S., Kamenetsky, V.S., Korsakov, A.V., Yaxley, G.M., 2018. Alkali-carbonate melts from the base of cratonic lithospheric mantle: Links to kimberlites. Chem. Geol. 483, 261–274. https://doi.org/10.1016/j.chemgeo.2018.02.016.

Green, D.H., 2015. Experimental petrology of peridotites, including effects of water and carbon on melting in the Earth's upper mantle. Phys. Chem. Miner. 42, 95–122. https://doi.org/10.1007/s00269-014-0729-2.

Guzmics, T., Mitchell, R.H., Szabó, C., Berkesi, M., Milke, R., Abart, R., 2011. Carbonatite melt inclusions in coexisting magnetite, apatite and monticellite in Kerimasi calciocarbonatite, Tanzania: melt evolution and petrogenesis. Contrib. Miner. Petrol. 161 (2), 177–196. https://doi.org/10.1007/s00410-010-0525-z.

Hogarth, D.D., 1997. Mineralogy of leucite-bearing dykes from Napoleon Bay, Baffin Island: multistage Proterozoic lamproites. Canad. Mineral 35, 53–78.

Hwang, P., Taylor, W.R., Rocky, N.M.S., Ramsay, R.R., 1994. Mineralogy, geochemistry and petrogenesis of the Metters Bore No. 1 lamproite pipe, Calwynyardah Field, West Kimberley Province, Western AustraliaMineralogie, geochemie und petrogenese der lamproit-pipe Metters Bore No. 1, Kalwynyardah Field, West Kimberley Provinz, West-Australien. Mineral. Petrol. 51 (2-4), 195–226.

Jaques, A.L., 2016. Major and trace element variations in oxide and titanate minerals in the West Kimberley lamproites, Western Australia. Mineral. Petrol. 110 (2–3), 159–197. https://doi.org/10.1007/s00710-015-0420-4.

Jaques, A.L., 2017. Major and trace element variations in oxide and titanate minerals in the West Kimberley lamproites, Western Australia. Mineral Petrol 110 (2–3), 159–197. https://doi.org/10.1007/s00710-015-0420-4.

Jaques, A.L., Lewis, J.D., Smith, C.B., 1986. The Kimberlites and Lamproites of Western Australia: Geological Survey West Australia. Bulletin 132:268.

Jaques, A.L., Foley, S.F., 1985. The origin of Al-rich spinel inclusions in leucite from the leucite lamproites of Western Australia. Amer. Mineral 70 (11–12), 1143–1150.

Jaques, A.L., Foley, S.F., 2018. Insights into the petrogenesis of the West Kimberley lamproites from trace elements in olivine. Mineral. Petrol. 112 (S2), 519–537. https://doi.org/10.1007/s00710-018-0612-9.

Jaques, A.L., Lewis, J.D., Smith, C.B., Gregory, G.P., Ferguson, J., Chappell, B.W., McCulloch, M.T., 1984a. The Diamond-Bearing Ultrapotassic (Lamproitic) Rocks of the West Kimberley Region, Western Australia. In: Kornprobst, J. (Ed.), Developments in Petrology, vol 11. Elsevier, pp. 225–254. https://doi.org/10.1016/B978-0-444-42273-6.50023-7.

Jaques, A.L., Webb, A.W., Fanning, C.M., Black, L.P., Pidgeon, R.T., Ferguson, J., Smith, C.B., Gregory, G.P., 1984b. The age of the diamond bearing pipes and associated leucite lamproites of the West Kimberley region, Western Australia. BMR J. Australian Geol. Geophys. 9, 1–7.

Jaques, A.L., Brink, F., Chen, J., 2020. Magmatic haggertyite in olivine lamproites of the West Kimberley region, Western Australia. Amer. Mineral. 105 (11), 1724–1733. https://doi.org/10.2138/am-2020-7456.

Kamenetsky, V.S., Kamenetsky, M.B., Sharygin, V.V., Faure, K., Golovin, A.V., 2007. Chloride and carbonate immiscible liquids at the closure of the kimberlite magma evolution (Udachnaya-East kimberlite, Siberia). Chem. Geol. 237 (3–4), 384–400. https://doi.org/10.1016/j.chemgeo.2006.07.010.

Kamenetsky, V.S., Grutter, H., Kamenetsky, M.B., Goemann, K., 2013. Parental carbonatitic melt of the Koala kimberlite (Canada): Constraints from melt

inclusions in olivine and Cr-spinel, and groundmass carbonate. Chem. Geol. 353, 96–111. https://doi.org/10.1016/j.chemgeo.2012.09.022.
Kamenetsky, V.S., Golovin, A.V., Maas, R., Giuliani, A., Kamenetsky, M.B., Weiss, Y., 2014. Towards a new model for kimberlite petrogenesis: Evidence from unaltered kimberlites and mantle minerals. Earth Sci. Rev. 139, 145–167. https://doi.org/10.1016/j.earscirev.2014.09.004.
Kamenetsky, M.B., Sobolev, A.V., Kamenetsky, V.S., Maas, R., Danyushevsky, L.V., Thomas, R., Pokhilenko, N.P., Sobolev, N.V., 2004. Kimberlite melts rich in alkali chlorides and carbonates: A potent metasomatic agent in the mantle. Geology 32 (10), 845–848. https://doi.org/10.1130/G20821.1.
Kent, A.J.R., 2008. Melt inclusions in basaltic and related volcanic rocks. Rev. Mineral. Geochem. 69, 273–331. https://doi.org/10.2138/rmg.2008.69.8.
Larsen, L.M., Rex, D.C., 1992. A review of the 2500 Ma span of alkaline-ultramafic, potassic and carbonatitic magmatism in West Greenland. Lithos 28, 367–402. https://doi.org/10.1016/0024-4937(92)90015-Q.
Lowenstern, J.B., 2003. Melt inclusions come of age: Volatiles, volcanoes, and sorby's legacy. In: De Vivo, B., Bodnar, R.J. (Eds.), Developments in Volcanology, vol 5. Elsevier, pp 1-21 https://doi.org/10.1016/S1871-644X(03)80021-9.
Lustrino, M., Agostini, S., Chalal, Y., Fedele, L., Stagno, V., Colombi, F., Bouguerra, A., 2016. Exotic lamproites or normal ultrapotassic rocks? The Late Miocene volcanic rocks from Kef Hahouner, NE Algeria, in the frame of the circum-Mediterranean lamproites. J. Volcanol. Geoth. Res. 327, 539–553. https://doi.org/10.1016/j.jvolgeores.2016.09.021.
Martin, L.H.J., Schmidt, M.W., Mattsson, H.B., Guenther, D., 2013. Element Partitioning between Immiscible Carbonatite and Silicate Melts for Dry and H2O-bearing Systems at 1–3 GPa. J. Petrol. 54 (11), 2301–2338. https://doi.org/10.1093/petrology/egt048.
Massare, D., Métrich, N., Clocchiatti, R.J.C.G., 2002. High-temperature experiments on silicate melt inclusions in olivine at 1 atm: inference on temperatures of homogenization and H_2O concentrations. Chem. Geol. 183 (1–4), 87–98. https://doi.org/10.1016/S0009-2541(01)00373-4.
Métrich, N., Wallace, P.J., 2008. Volatile abundances in basaltic magmas and their degassing paths tracked by melt inclusions. Rev. Mineral. Geochem. 69, 363–402. https://doi.org/10.2138/rmg.2008.69.10.
Mitchell, R.H., 1991. Coexisting glasses occurring as inclusions in leucite from lamproites: examples of silicate liquid immiscibility in ultrapotassic magmas. Mineral. Mag. 55, 197–202. https://doi.org/10.1180/minmag.1991.055.379.07.
Mitchell, R.H. (Ed.), 1995a. Kimberlites, Orangeites, and Related Rocks. Springer US, Boston, MA.
Mitchell, R.H., 1995b. Melting Experiments on a Sanidine Phlogopite Lamproite at 4–7 GPa and their Bearing on the Sources of Lamproitic Magmas. J. Petrol. 36 (5), 1455–1474. https://doi.org/10.1093/petrology/36.5.1455.
Mitchell, R.H., 2020. Igneous Rock Associations 26. Lamproites, Exotic Potassic Alkaline Rocks: A Review of their Nomenclature, Characterization and Origins. Geosci. Can. 47 (3), 119–142 10.12789/geocanj.2020.47.162.
Mitchell, R.H., Bergman, S.C. (Eds.), 1991. Petrology of Lamproites. Springer US, Boston, MA.
Mitchell, R.H., Fareeduddin, 2009. Mineralogy of peralkaline lamproites from the Raniganj Coalfield, India. Mineral Mag 73 (3), 457–477.
Moussallam, Y., Morizet, Y., Massuyeau, M., Laumonier, M., Gaillard, F., 2014. CO_2 solubility in kimberlite melts. Chem. Geol. 418, 198–205. https://doi.org/10.1016/j.chemgeo.2014.11.017.
Moussallam, Y., Morizet, Y., Gaillard, F., 2016. H_2O–CO_2 solubility in low SiO2-melts and the unique mode of kimberlite degassing and emplacement. Earth Planet. Sci. Lett. 447, 151–160. https://doi.org/10.1016/j.epsl.2016.04.037.
Ngwenya, N.S., Tappe, S., 2021. Diamondiferous lamproites of the Luangwa Rift in central Africa and links to remobilized cratonic lithosphere. Chem. Geol. 568,. https://doi.org/10.1016/j.chemgeo.2020.120019 120019.
Oliver, B.G., Davis, A.R., 1973. Vibrational spectroscopic studies of aqueous alkali metal bicarbonate and carbonate solutions. Can. J. Chem. 51, 698–702. https://doi.org/10.1139/v73-106.
Pan, V., Holloway, J.R., Hervig, R.L., 1991. The pressure and temperature dependence of carbon dioxide solubiliy in tholeiitic basalt melts. Geochim. Cosmochim. Acta 55, 1587–1595. https://doi.org/10.1016/0016-7037(91)90130-W.
Panina, L.I., 2005. Multiphase carbonate-salt immiscibility in carbonatite melts: data on melt inclusions from the Krestovskiy massif minerals (Polar Siberia). Contrib. Miner. Petrol. 150 (1), 19–36. https://doi.org/10.1007/s00410-005-0001-3.
Panina, L.I., Motorina, I.V., Usol'tseva, L.M., 1998. Genesis of the Cocites of North Vietnam Based on Melt Inclusion Study. Geol. Geofiz. 39(7), 882–891.
Panina, L.I., Konev, A.A., 1995. Genetic Features of the Lamproites of the Molbo River (Western Aldan). Geokhimiya 3, 366–376.
Panina, L.I., Motorina, I.V., 2008. Liquid immiscibility in deep-seated magmas and the generation of carbonatite melts. Geochem. Int. 46 (5), 448–464. https://doi.org/10.1134/S0016702908050029.
Panina, L.I., Usol'tseva, L.M., 1999. Alkaline High-Ca Sulfate-Carbonate Melt Inclusions in Melilite–Monticellite–Olivine Rocks from the Malomurunskii Alkaline Massif, Aldan. Petrologiya 7, 653–669.
Panina, L.I., Usol'tseva, L.M., Vladykin, N.V., 1996. Lamproite rocks of the Yakokutsk Massif and Upper Yakokutsk Depression. Geolog geofiz 37 (6), 16–26.
Panina, L.I., Usol'tseva, L.M., 2000. Role of Liquid Immiscibility in the Formation of Calcite Carbonatites of the Malyi Murun Massif (Aldan). Geolog geofiz 41 (5), 665–670.
Panina, L.I., Vladykin, N.V., 1994. Lamproite rocks of the Murunsky Massif and their genesis. Geologi geofiz 12, 100–113.
Pearson, D.G., Woodhead, J., Janney, P.E., 2019. Kimberlites as Geochemical Probes of Earth's Mantle. Elements 15 (6), 387–392. https://doi.org/10.2138/gselements.15.6.387.
Perrin, J., Vielzeuf, D., Laporte, D., Ricolleau, A., Rossman, G.R., Floquet, N., 2016. Raman characterization of synthetic magnesian calcites. Am. Mineral. 101, 2525–2538. https://doi.org/10.2138/am-2016-5714.
Phillips, D., Clarke, W. Jaques, A.L., 2012. New 40Ar/39Ar ages for the West Kimberley lamproites and implications for Australian plate geodynamics. In International Kimberlite Conference: Extended Abstracts, Vol. 10.
Prelević, D., Stracke, A., Foley, S.F., Romer, R.L., Conticelli, S., 2010. Hf isotope compositions of Mediterranean lamproites: Mixing of melts from asthenosphere and crustally contaminated mantle lithosphere. Lithos 119, 297–312. https://doi.org/10.1016/j.lithos.2010.07.007.
Prider, R.T., 1939. Some minerals from the leucite-rich rocks of the West Kimberley area, Western Australia. Mineral. Magaz. J. Mineral. Soc. 25 (166), 373–387. https://doi.org/10.1180/minmag.1939.025.166.01.
Prider, R.T., 1959. The leucite lamproites of the Fitzroy Basin, Western Australia. J. Geol. Soc. Aust. 6 (2), 71–118. https://doi.org/10.1080/00167615908728501.
Roedder, E., 1984. Fluid Inclusions. In: Reviews in Mineralogy & Geochemistry 12 Book Crafters Inc., Michigan https://doi.org/10.1515/9781501508271.
Rokosova, E.Y., Panina, L.I., 2013. Shonkinites and minettes of the Ryabinovyi massif (Central Aldan): composition and crystallization conditions. Russ. Geol. Geophys. 54 (6), 613–626. https://doi.org/10.1016/j.rgg.2013.04.011.
Ryabchikov, I., Solovova, I.P., Sobolev, N.V., Sobolev, A., Bogatikov, O.A., Aleshin, B.G., Vashchenko, A.N., 1986. Nitrogen in lamproite magmas. Geochimica 553.21 + 553.24:976-979.
Salvioli-Mariani, E., Toscani, L., Bersani, D., 2004. Magmatic evolution of the Gaussberg lamproite (Antarctica): volatile content and glass composition. Mineral. Mag. 68 (01), 83–100. https://doi.org/10.1180/0026461046810173.
Salvioli-Mariani, E., Venturelli, G., 1996. Temperature of crystallization and evolution of the Jumilla and Cancarix lamproites (SE Spain) as suggested by melt and solid inclusions in minerals. Eur. J. Mineral. 8 (5), 1027–1040.
Scheetz, B.E., White, W.B., 1977. Vibrational spectra of the alkaline earth double carbonates. Am. Mineral. 62, 36–50.
Schmidt, B.C., Gehlken, P.-L., Böttcher, M.E., 2013. Vibrational spectra of BaMn(CO3) 2 and a re-analysis of the Raman spectrum of BaMg(CO3)2. Eur. J. Mineral. 25, 137–144. https://doi.org/10.1007/s00269-019-01038-w.
Sergreev, S., Lobach-Zhuchenko, S., Larianov, A., Berezhenya, N., Guseva, N., 2007. Archaean age of miaskite lamproites from the Panozero Complex, Karelia. Dodklady Earth Sci. A 413, 420–423. https://doi.org/10.1134/S1028334X07030221.
Sharygin, V.V., 1991. Chemical composition of melt inclusions in lamproite minerals, Ellendale field, Western Australia. Geol. Geofiz 32, 54–61.
Sharygin, V., 1997. Evolution of lamproites suggested by melt inclusions in minerals. Geol. Geofiz 38 (1), 142–153.
Sharygin, V.V., Bazarova, T., 1991. Melt evolution features during crystallization of wyomingites, Leucite Hills, USA. Geol. Geofiz 32 (6), 51–57.
Sharygin, V., Panina, L.I., Vladykin, N.V., 1998. Melt inclusions in minerals from lamproites of Smoky Butte, (Montana, USA). Geol. Geofiz 39 (1), 35–51.
Smith, C., 1983. Pb, Sr and Nd isotopic evidence for sources of southern African Cretaceous Kimberlites. Nature 304, 51–54. https://doi.org/10.1038/304051a0.
Smith, C.G., Lorenz, V., 1989. Volcanology of the Ellendale lamproite pipes, Western Australia. Western Australia. Proc. 4th Int. Kimb. Conf., Perth. Geol. Soc. of Australia Spec. Pub., No. 14, 505–519
Sobolev, V., Bazarova, T., Yagi, K., 1975. Crystallization temperature of wyomingite from Leucite Hills. Contrib. Miner. Petrol. 49, 301–308. https://doi.org/10.1007/BF00376182.
Sobolev, A.V., Sobolev, N.V., Smith, C.B., Kononkova, N.N., 1985. A new data on the petrology of olivine lamproites, Western Australia based on the study of magmatic inclusions in olivine. Dokladi Academia Nauk USSR 284 (196–201).
Sobolev, A., Sobolev, N., Smith, C., Dubessy, J., 1986. Peculiarities in the fluid and melt compositions of the lamproites and kimberlites based on the study of inclusions in olivines. International Kimberlite Conference: Extended Abstracts 4, 93–94 10.29173/ikc1084.
Sobolev, A.V., Sobolev, N.V., Smith, C.B., Dubessy, J., 1989. Fluid and melt compositions in lamproites and kimberlites based on the study of inclusions in olivine. In: Ross, J. (Ed.), 4-th International Kimberlite Conference, Kimberlites and Related Rocks V1 Their composition, occurrences, origin and emplacement. Blackwell Sci Publ, Perth, pp. 220–240.
Solovova, I., Kogarko, L., Ryabchikov, I., Naumov, V., Girnis, A., Kononkova, N., Venturelli, G., 1988. Spanish high-potassium magmas and evidence of their generation depth (as inferred from thermobarogeochemical data). In: Transactions (Doklady) of the USSR Academy of Sciences Earth Science Sections, vol 303. pp 100-103.
Solovova, I.P., Girnis, A.V., Kogarko, L.N., Ryabchikov, I.D., Naumov, V.B., Guzhova, A.V., 1989. Geochemical Features of the Prairie Creek Lamproites Based on the Investigation of Microinclusions in Olivines. Geokhimiya 10, 1449–1459.
Stachel, T., Lorenz, V., Smith, C., Jaques, A., 1994. Evolution of four individual lamproite pipes, Ellendale Volcanic Field (Western Australia). In book: Kimberlites, Related Rocks and Mantle Xenoliths (Proceedings of the 5th International Kimberlite Conference)Publisher: CPRM, Rio de Janeiro, BrasilEditors: Henry O. A. Meyer, Othon H. Leonardos pp. 177-194.
Stolper, E., Holloway, J.R., 1988. Experimental determination of the solubility of carbon dioxide in molten basalts at low pressure. Earth Planet. Sci. Lett. 87, 397–408. https://doi.org/10.1016/0012-821X(88)90004-0.

Tappe, S., Foley, S.F., Stracke, A., Romer, R.L., Kjarsgaard, B.A., Heaman, L.M., Joyce, N., 2007. Craton reactivation on the Labrador Sea margins: 40Ar/39Ar age and Sr–Nd–Hf–Pb isotope constraints from alkaline and carbonatite intrusives. Earth Planet. Sci. Lett. 256, 433–454. https://doi.org/10.1016/j.epsl.2007.01.036.

Tappe, S., Foley, S.F., Kjarsgaard, B.A., Romer, R.L., Heaman, L.M., Stracke, A., Jenner, G.A., 2008. Between carbonatite and lamproite—Diamondiferous Torngat ultramafic lamprophyres formed by carbonate-fluxed melting of cratonic MARID-type metasomes. Geochim. Cosmochim. Acta 72, 3258–3286. https://doi.org/10.1016/j.gca.2008.03.008.

Tappe, S., Shaikh, A.M., Wilson, A.H., Stracke, A., 2022. Evolution of ultrapotassic volcanism on the Kaapvaal craton: deepening the orangeite versus lamproite debate. Geological Society, London, Special Publications 513, 17–44. https://doi.org/10.1144/SP513-2021-84.

Thibault, Y., Holloway, J.R., 1994. Solubility of CO_2 in a Ca-rich leucitite: effects of pressure, temperature, and oxygen fugacity. Contrib. Miner. Petrol. 116 (1), 216–224. https://doi.org/10.1007/BF00310701.

Thomas, R., Davidson, P., Schmidt, C., 2011. Extreme alkali bicarbonate- and carbonate-rich fluid inclusions in granite pegmatite from the Precambrian Rønne granite, Bornholm Island, Denmark. Contrib. Miner. Petrol. 161, 315–329. https://doi.org/10.1007/s00410-010-0533-z.

Thy, P., Stecher, O., Korstgård, J.A., 1987. Mineral chemistry and crystallization sequences in kimberlite and lamproite dikes from the Sisimiut area, central West Greenland. Lithos 20, 391–417. https://doi.org/10.1016/0024-4937(87)90018-1.

Tingey, R.J., McDougall, I., Gleadow, A.J.W., 1983. The age and mode of formation of Gaussberg, Antarctica. J. Geol. Soc. Aust. 30, 241–246. https://doi.org/10.1080/00167618308729251.

Trussov, I.A., Kokhmetova, S.T., Driscoll, L.L., Smith, R., Berry, F.J., Marco, J.F., Galeyeva, A.K., Kurbatov, A.P., Slater, P.R., 2020. Synthesis, structure and electrochemical performance of Eldfellite, NaFe(SO4)2, doped with SeO4, HPO4 and PO3F. J. Solid State Chem. 289,. https://doi.org/10.1016/j.jssc.2020.121395 121395.

Venturelli, G., Capedri, S., Barbieri, M., Toscani, L., Salvioli Mariani, E., Zerbi, M., 1991. The Jumilla lamproite revisited: a petrological oddity. Eur. J. Mineral. 3 (1), 123–146.

Venturelli, G., Salvioli-Mariani, E., Toscani, L., Barbieri, M., Gorgoni, C., 1993. Post-magmatic apatite + hematite + carbonate assemblage in the Jumilla lamproites. A fluid inclusion and isotope study. Lithos 30 (2), 139–150. https://doi.org/10.1016/0024-4937(93)90012-2.

Wade, A., Prider, R.T., 1940. The leucite-bearing rocks of the West Kimberley area, Western Australia. Quart. J. Geol. Soc. 96 (1-4), 39–NP.

Wellman, P., 1973. Early Miocene potassium-argon age for the Fitzroy Lamproites of Western Australia. J. Geol. Soc. Aust. 19 (4), 471–474. https://doi.org/10.1080/00167617308728815.

Zaitsev, A.N., 2010. Nyerereite from calcite carbonatite at the Kerimasi Volcano, Northern Tanzania. Geol. Ore Deposits 6, 630. https://doi.org/10.1134/S1075701510070159.

Zucchini, A., Gavryushkin, P.N., Golovin, A.V., Bolotina, N.B., Stabile, P., Carroll, M.R., Comodi, P., Frondini, F., Morgavi, D., Perugini, D., Arzilli, F., Cherin, M., Kazimoto, E., Kokh, K., Kuznetsov, A., Medrish, I.V., 2022. The nyerereite crystal structure: a possible messenger from the deep Earth. Am. Mineral. https://doi.org/10.2138/am-2022-8106. In Press.